INORGANIC AND ORGANIC CARBON VARIATIONS IN SURFACE WATER, KONZA PRAIRIE LTER SITE, USA, AND MAOLAN KARST EXPERIMENTAL SITE, CHINA

By

HUAN LIU

Submitted to the graduate degree program in Geology and the Graduate Faculty of the University of Kansas in partial fulfillment of the requirements for the degree of Master of Science.

_____

Chairperson Gwendolyn L. Macpherson

_____

Luis González

_____

Jennifer Roberts

_____

Daniel Hirmas

_____

Randy Stotler

Date Defended: 27/01/2014

The Thesis Committee for Huan Liu
certifies that this is the approved version of the following thesis:

INORGANIC AND ORGANIC CARBON VARIATIONS IN SURFACE WATER, KONZA PRAIRIE LTER SITE, USA, AND MAOLAN KARST EXPERIMENTAL SITE, CHINA

_____
Chairperson Gwendolyn L. Macpherson

Date approved: 27/01/2014

**ABSTRACT**

Two natural groundwater-fed streams were selected to examine the diurnal trends of water geochemistry, $CO_2$ emissions, and sources of OC on 25 May 2012 at the Konza Prairie Long-Term Ecological Research (LTER) site, USA and 29 August – 30 August 2012 at the Maolan Karst Experimental (Maolan) Site, China.

For the stream at the Konza LTER site, little variation in water chemistry was observed among the upstream, midstream and downstream locations, indicating the groundwater and stream water chemistry was mostly stable on a daily basis. $\delta^{13}C_{DIC}$ was the highest at the downstream site due to the largest $CO_2$ degassing. The autochthonous particulate organic carbon (POC) fraction at the upstream, midstream and downstream sites was 12-35%, 39-65% and 75-88%, respectively. Estimation of the C/N ratio for POC samples at the three locations was 10.4-15.0, 14.0-15.9 and 12.2-13.3. This is comparable to previously measured C/N ratios of suspended POC.

For the stream at the Maolan site, there was little or no diel variation in the spring water physical and chemical parameters. However, all parameters show distinct diel changes in the spring-fed midstream pond with flourishing submerged plants. Temperature, pH, DO, $SI_C$, $\delta^{13}C_{DIC}$ increased during the day and decreased at night, while EC, $[HCO_3^-]$, $[Ca^{2+}]$, and $pCO_2$ behaved in the opposite sense. Strong aquatic photosynthesis was indicated from maximum DO values (two to three times higher than normal water equilibrated with atmospheric $O_2$). In the downstream pond with fewer submerged plants but larger volume, all parameters displayed similar trends to the midstream pond but with much less change. We attribute this pattern to the lower biomass/water volume ratio. The diel variations in the two ponds resulted from the aquatic photosynthetic effect, demonstrating that natural surface water systems may constitute an important sink of carbon.

**ACKNOWLEDGEMENTS**

I would like to express my greatest appreciation to my scientific supervisor Dr. Gwendolyn L. Macpherson for her patient guidance, and encouragement during my study at The University of Kansas. I am inspired by her tremendous expertise, constant enthusiasm, rigorous attitude towards academic research. The thesis could not have been completed without her supervision and assistance.

I would also like to sincerely thank the University of Kansas geology faculty Dr. Luis Gonzales, Dr. Jennifer Roberts, Dr. Daniel Hirmas, and Dr. Randy Stotler for valuable instructions. I am very grateful to Greg Cane for his support with the lab work at KU and Dr. Andrea Brookfield for taking the thermal images in the field at Konza.

Special thanks are given to Dr. Zaihua Liu for his thoughtful comments and suggestions, which greatly improved the original Chapter 3 draft. Dr. Rui Yang, Dr. Hailong Sun and Chen Bo are very much appreciated for their help in lab and field work in China.

This work was supported by the KU Department of Geology research grant, the Konza Prairie LTER Program, and the 973 Program of China (2013CB956703).

**TABLE OF CONTENTS**

# CHAPTER 1. GENERAL INTRODUCTION

This master thesis is based on the field data collected on 25 May 2012 at the Konza Prairie Long-Term Ecological Research (LTER) site, and 29 August – 30 August 2012 at the Maolan Karst Experimental Site. Laboratory analyses were performed in the University of Kansas and State Key Laboratory of Environmental Geochemistry facilities in cooperation with the faculty and stuff of the Department of Geology and Chinese Academy of Science.

The purpose of this work was to incorporate measurements of the physical and chemical parameters in groundwater-fed surface water to understand the underlying mechanisms causing the daily differences. This work evaluates the contribution of dissolved inorganic carbon to organic carbon and the $CO_2$ gas exchange between water and atmosphere.

Chapter 2 and 3 describe slightly different focuses on the similar aspect of the thesis work in two natural carbonate terrains. Each of the two chapters contains a summary, introduction, location, methods, results, discussion, and conclusions. The appendices provide more details about the sampling, methods and additional information and data not included in those chapters. The long-term data analysis of groundwater geochemistry at Konza Prairie is also in the appendices.

Chapter 2 discusses the processes influencing $CO_2$ emissions from a $5^{th}$-order groundwater-fed stream at the Konza Prairie LTER site, USA. Direct $CO_2$ outgassing rate from the stream water is measured using the floating chamber approach. The measured fluxes are compared with fluxes calculated from the lake gas transfer velocity. Thermal imaging is used to verify that groundwater is discharged to the stream. The fluxes are also used to estimate the fraction of transformation of dissolved inorganic carbon (DIC) into organic carbon using stable carbon isotopes; the C/N ratio of POC, calculated using the same fraction, is compared to previously measured POC, and so is an independent verification of the calculations.

Chapter 3 reveals the underlying mechanisms of diel spatiotemporal differences in groundwater-fed ponds at the Maolan Karst Experimental Site, China. It characterizes the water geochemistry and stable carbon isotopes in three ponds. The dominating factors (including groundwater input, water temperature, gas exchange, biological processes and calcite dissolution/precipitation) controlling the daily spatiotemporal variations are proposed. $CO_2$ efflux/influx is examined using the floating chamber approach. The daily organic carbon formation is quantified.

Inland freshwater ecosystems are parts of the terrestrial landscape, but they have not yet been included in the terrestrial greenhouse gas balance. This study shows reasons to consider groundwater and surface water as one of the missing carbon sinks in the global carbon budget and provides a valuable tool for improving input to quantification of the global carbon cycle.

# CHAPTER 2. SOURCES OF ORGANIC CARBON IN A STREAM, KONZA PRAIRIE LONG-TERM ECOLOGICAL RESEARCH SITE, USA

**Chapter summary**

Inland freshwater ecosystems (mainly rivers, lakes, and reservoirs) play a significant role in the global and regional carbon cycle because organic carbon (OC) formed during aquatic photosynthesis incorporates dissolved inorganic carbon (DIC). DIC may be sourced from chemical weathering of carbonates; thus, carbonates may play a role in sequestration of atmospheric or groundwater $CO_2$ in the long run. In this study, a tributary stream in a carbonate-rich terrain at the Konza Long-Term Ecological Research (LTER) site, USA, was selected to study the sources and dynamics of DIC and OC.

Water samples and $CO_2$ samples were taken at three locations from upstream to downstream on 25 May under cloudy/sunny weather. The stream water level was lower than the mean daily statistic. Infrared images show colder groundwater discharging into warmer stream water from the stream channel side and bottom at all three locations. The pH ranged from 7.1 to 7.4. The temperature of downstream location was the highest (19.9$^{o}$C). DO ranged from 4.7 mg/L (upstream) to 6.1 mg/L (downstream). DO% was highest at the downstream site. $\delta^{13}C_{DIC}$ was the highest at the downstream site and resulted from the largest $CO_2$ outgassing. There was little variation in the other parameters among the three locations indicating the groundwater and stream water chemistry was mostly stable during midday.

$\delta^{13}C$ of soil samples, POC samples, aquatic and terrestrial plant samples were determined in order to calculate the autochthonous fraction. The estimated percentage of autochthonous carbon in POC at the upstream, midstream and downstream sites is 12-35%, 39-65% and 75-88%, respectively. However, the overall aquatic photosynthesis at Konza was not strong due to the lack of submerged plants, also evidenced by low DO.

## 1. Introduction

The long-term carbon cycle (Berner, 2004) is driven by weathering of silicate minerals, which sequesters $CO_2$:

$$CO_2 + CaSiO_3 = CaCO_3 + SiO_2 \quad (1)$$

In limestone-dominated terrains, weathering of carbonate minerals:

$$CO_2 + H_2O + CaCO_3 = Ca^{2+} + 2HCO_3^- \quad (2)$$

is thought to provide only very short-term sequestration of $CO_2$, because of the reversal of chemical reaction (2), either locally or when fresh water mixes with seawater. Recent studies show that the transformation of dissolved inorganic carbon (DIC) to organic carbon (OC) by terrestrial photosynthetic aquatic organisms (Liu et al., 2010; Liu et al., 2011) is an important carbon sink when this OC is buried and stored. In this case, the reverse of equation (2) becomes:

$$Ca^{2+} + 2HCO_3^- = CaCO_3 + \phi\,(CO_2 + H_2O) + (1 - \phi)\,(CH_2O + O_2) \quad (3)$$

where $\phi$ is the fraction of inorganic carbon partitioned to $CO_2$, and $1-\phi$ is the fraction of carbon partitioned to organic carbon through photosynthesis. The OC here includes both DOC and particulate organic carbon (POC) and, in equation (3), $CH_2O$ is used to represent OC. This work focuses on POC since it may contribute to the longer-term storage.

POC in stream water and stream sediments may be sourced from eroded soil organic carbon (Billings et al., 2010), eroded or fallen above-ground plant litter (allochthonous), or aquatic primary production (autochthonous) (Downing et al., 2008). Stable carbon isotopes have been successfully applied as a useful tool for determining POC sources. Carbon stable isotopes are expressed in units of per mil, using the ratio (R) of the heavy to light C stable isotopes, $^{13}C/^{12}C$.

$$\delta^{13}C_{sample} = ((R_{sample}/R_{standard}) - 1) * 1000 \quad (4)$$

Aquatic plants are generally enriched in $^{12}C$ when compared with terrestrial plants due to different fractionation mechanisms (Mook and Tan, 1991). Terrestrial C4 plants have higher carbon isotope ratios than C3 plants (Farquhar et al., 1982). Therefore, the $\delta^{13}C$ of POC can potentially differentiate between C sourced from aquatic plants, terrestrial plants, soils and/or groundwater. However, if the carbon isotope composition of different carbon pools overlap with each other, an additional discriminant, such as C/N ratio (Tao et al., 2009; Sun et al., 2011), can be used in conjunction with carbon isotope ratios.

## 2. Setting

The Konza Long Term Ecological Research Site (Konza) is a 3487 ha tallgrass prairie located in the Flint Hills region of northeastern Kansas, about 10 km south of Manhattan, Kansas. The Flint Hills region encompasses over 1.6 million ha extending throughout much of eastern Kansas from near the Kansas-Nebraska border south into northeastern Oklahoma, and contains the largest remaining area of unplowed tallgrass prairie in North America. Konza is an unplowed native tallgrass prairie. The vegetation is mostly perennial, warm-season C4 grasses, predominately big bluestem, little bluestem, Indiangrass and switchgrass. Less abundant species include warm-season and cool-season grasses, composites, legumes, and other forbs. Riparian zones are mostly wooded in lower stream reaches and prairie in the uppermost stream reaches (www.konza.ksu.edu).

The bedrock at Konza is composed of Early Permian couplets of limestone and shale. The 1 – 2 m thick limestone layers and the alluvial deposits act as aquifers at this site. Konza prairie soils are developed on loess, limestone and shale, and are generally less than 1 m thick (Macpherson et al., 2008). Soils are usually carbonate-poor, with moderate to low cation exchange capacities (mostly < 40 $cmol_c/kg$) (Ransom et al., 1998).

The climate of Konza prairie is temperate mid-continental climate. Yearly mean temperature is 13 ℃. Average monthly temperature ranges from 2.7 ℃ in January to 26.6 ℃ in July. Average total annual precipitation is 835 mm with 75% falling during the growing season – April through October; May and June are months with the highest average precipitation (www.konza.ksu.edu).

The sampling site is Kings Creek, which drains 10.6 $km^2$ of grassy terrain in the Flint Hills (fig. 2.1); the drainage area of Kings Creek above the sampling site is entirely within the boundaries of the Konza LTER site, and thus protected from contamination unless it is airborne. Kings Creek is tributary to McDowell Creek, which drains into the Kansas River.

Kings Creek is an intermittent stream with sustained flows generally occurring in the spring. Stream flow usually ceases during late summer and remains dry during the fall. Flow in headwater channels occurs only immediately following rainfall events (Mast and Turk, 1999). Mean monthly discharges range from less than 0.01 $m^3/s$ in September to 0.23 $m^3/s$ in May, and average annual runoff is about 20 cm (Putnam et al., 1996). Stream water in Kings Creek is a calcium bicarbonate type. Kings Creek is a USGS Benchmark Stream, and based on quarterly chemical analyses from 1982 to 1995, the total ion concentrations ranged from 4,300 to 14,000 meq/L. Alkalinity ranged from 1,900 to 6,200 meq/L, and bicarbonate was the primary contributor to alkalinity. The most abundant cation is calcium, contributing 73% of median cation concentration. The most abundant anion is bicarbonate at 87% of the median anion concentration (Mast and Turk, 1999). The ion composition of the stream water results from the weathering of the underlying limestone bedrock (Mast and Turk, 1999) or from a combination of bedrock limestone weathering and weathering of a solid with more radiogenic $^{87}Sr/^{86}Sr$ than the limestone (Wood and Macpherson, 2005).

## 3. Methods

### 3.1. Field Procedures

The field sampling occurred on 25 May 2012. This is normally the wet season of the year, but 2012 was exceptional in that the discharge rate of Kings Creek was about 56.6 L/s lower than the median daily statistic of 33 years (fig. 2.2). We collected water samples from three locations on Kings Creek, here called upstream, midstream and downstream. Based on the GPS coordinates, the distance between upstream and midstream locations is about 22 m, and about 26 m between midstream and downstream locations. At each sampling location, water in the center of the stream was collected 5 cm above the bottom for parts deeper than 10 cm and near the bottom for parts shallower than 10 cm. Samples for C/N of POC and $\delta^{13}C_{POC}$ were each collected into two pre-cleaned 2 L HDPE bottles and poisoned with saturated $HgCl_2$ immediately after collection. On that day, these water samples were filtered through pre-weighted, pre-ashed (500 ℃, 5h) 47 mm Whatman GF/F glass fiber filters (0.65 μm). A two-liter sample in a pre-cleaned HDPE temporary collection bottle was placed immediately on ice, and filtered in the field-station laboratory through 0.45 μm filters into three containers. The first was a pre-cleaned 30-mL glass vial for determination of $\delta^{13}C_{DIC}$ that was filled from the bottom until there was no air space. The next two were pre-cleaned 250 mL LDPE bottles. One of the two 250 mL bottles was filled so no air space remained and used for anion determination, including alkalinity. The other, pre-weighed, was filled to approximately 250 mL, weighed in the lab, and concentrated nitric acid added at a volume proportion of 1:50 (acid:sample) for preservation of cations. All liquid samples were stored in a cold environment ($4^oC$) until analyzed.

Samples for terrestrial (vegetation and soil) and aquatic carbon were collected for $\delta^{13}C$ and C/N content. At each site, leaves from 10 land plant samples were collected for $\delta^{13}C$ analysis and used to approximate the $\delta^{13}C$ of terrestrial C3 and C4 plants. The previously measured OC

$\delta^{13}C$ at Konza (Johnson et al., 2007) would serve as a test of the validity of this approximation. Three soil samples from each site (from 0~45 cm depth) were collected using a shallow depth Backsaver® soil sampler to establish a representative C/N and $\delta^{13}C$ for soil organic matter. Three samples of submerged aquatic plants were collected and analyzed to establish the aquatic isotopic signature of $\delta^{13}C$.

Unstable parameters (pH; temperature; dissolved oxygen, DO; Eh) were measured on site in a beaker using individual probes and meters.

A floating $CO_2$ chamber was placed on the surface of the waters to collect $CO_2$ efflux from the stream (details in section 4.c, below). Five $CO_2$ samples were taken at an interval of approximately 1-min at each location.

### 3.2. Laboratory Procedures

*Sample treatment:* The glass-fiber filters were freeze-dried for POC, C/N and $\delta^{13}C$ analyses. They were then acidified with dilute HCl and oven-dried overnight at 105 ℃ and weighed prior to analysis. A portion of the filter paper was cut and loaded into a 9 x 10 mm tin capsule. Terrestrial and aquatic plant samples were washed under DI water to get rid of dust/soil; oven-dried for 2-3 days at 46$^{o}$C and grinded using a mortar and pestle with liquid nitrogen added. Roots in the soil samples were picked out and soil samples were dried overnight and weighted; acidified with 0.5 M HCl.

*Laboratory analyses*: The C/N content and $^{13}C$ was determined on a Costech ECS 4010 elemental analyzer and a dual-inlet isotope ratio mass spectrometer (ThermoFinnigan MAT 253 Dual Inlet System), respectively at the W. M. Keck Paleoenvironmental and Environmental Stable Isotope Laboratory (Dept. of Geology). Alkalinity was determined by titration with ~0.02 N $H_2SO_4$, with the titration end point determined as the maximum slope of the titration curve in

the vicinity of pH 4.5. Other major anion concentrations (Cl, $NO_3$-N, $SO_4$) were determined by ion chromatography (KU Aqueous Geochemistry Lab, Dept. of Geology). Cation concentrations (Ca, Mg, Na, K, Sr, B, Ba, Li, Si, F) were determined by ICP-OES (KU Plasma Analytical Laboratory, Dept. of Geology).

### 3.3. Calculations

The fraction of autochthonous and allochthonous POC can be quantified by considering their $\delta^{13}C$ values as end-members in a mass balance:

$$^{13}C_{sample} = X * \delta^{13}C_{au} + (1-X) * \delta^{13}C_{al} \quad (5)$$

$$(C/N)_{sample} = Y * (C/N)_{au} + (1-Y) * (C/N)_{al} \quad (6)$$

In these equations, "au" is subscript for autochthonous and "al" is subscript for allochthonous. The data from POC in stream waters will be used for $^{13}C_{sample}$. X and Y are the fraction of the autochthonous POC calculated from (5) and (6) based on $\delta^{13}C$ and C/N. 1-X and 1-Y are the fractions of allochthonous POC. Theoretically, for the proportion of autochthonous POC, X = Y, and for the proportion of allochthonous POC, 1-X = 1-Y.

DIC, calcite saturation and $pCO_2$ were calculated using the geochemical speciation model PHREEQC Interactive 2.18.5570, with the PHREEQC database (Parkhurst and Appelo, 1999.) Precise pH measurements are critical for determining carbonate system equilibria (Langmuir, 1971). We used field-measured pH and temperature along with laboratory-determined alkalinity (prior work at this site shows alkalinity in filtered, cooled samples does not change for at least two weeks after sample collection; Macpherson, unpublished data), other anions, and cations. The excellent charge balances on the samples collected (-0.00031~ -0.00029) support use of laboratory-determined measurements.

## 4. Results

### 4.1. Physical chemistry of the stream water

Fig. 2.3 shows colder groundwater discharging into warmer stream water from the side and bottom of the stream channel. From the infrared image (fig. 2.3a) that was taken from a position near the midstream location, the groundwater temperature was around 18.3 ˚C at the time the image was captured. Table 2.1 shows the physical chemistry of the upstream, midstream and downstream water, sampled in that order. The temperature of the downstream-site water was the highest (19.9 ˚C); the air temperature also increased during the sampling from 21 ℃ to 23 ℃ over the entire sampling day. DO ranged from 4.7 mg/L at the upstream site to 6.1 mg/L at the downstream site. The DO% was also the highest at the downstream site. $\delta^{13}C_{DIC}$ was highest at the downstream site and lowest at the midstream site. There was little variation in the other parameters among the three locations. The pH ranged from 7.1 to 7.4, SC varied from 637 μs/cm to 643 μs/cm, averaging 640 μs/cm. Eh changed from 194 mv to 198 mv. The alkalinity, at an average of 383 mg/L, is typical of water in limestone aquifers. Calculated $CO_2$ values from PHREEQC for the upstream, middle and downstream sites were 16800 ppmv, 26800 ppmv and 13400 ppmv, respectively.

### 4.2. $\delta^{13}C$ and C/N for the soil, plant and POC samples

Table 2.2 shows that $\delta^{13}C$ and C/N of soil samples ranged from -20.40‰ to -18.56‰, and 10.5 to 11.0, respectively. $\delta^{13}C$ and C/N of terrestrial plant samples ranged from -31.19‰ to -26.96‰, and 14.6 to 82.9. $\delta^{13}C$ and C/N of aquatic plant samples ranged from -35.90‰ to -29.96‰, and 9.4 to 15.9. $\delta^{13}C$ of POC samples was the lowest at downstream site (-28.58‰) and highest at upstream (-25.86‰). The C/N values of POC samples could not be measured because of the low N content.

### 4.3. $CO_2$ efflux

Fig. 2.4, Fig. 2.5 and Table 2.3 present the results from the $CO_2$ floating chamber. $CO_2$ was the highest at the downstream site: the initial $CO_2$ concentration in the chamber was 456 ppmv and increased to 508 ppmv after a measuring period of 175 seconds. At the upstream site, the $CO_2$ concentration started at 404 ppmv and increased to 462 ppmv after 220 seconds. At the midstream site, $CO_2$ concentration began at 424 ppmv and increased to 457 ppmv after 155 seconds. Estimated $CO_2$ fluxes (Table 2.4a) for the three sites were 7900, 5400 and 7500 $mg/d/m^2$ at the upstream, midstream and downstream sites, respectively. The $\delta^{13}C$ of $CO_2$ in the chamber decreased from -9.50‰ to -10.03‰ for the upstream site, while for midstream and downstream sites, $\delta^{13}C_{CO2}$ decreased from -9.14‰ to -9.87‰, and -10.47‰ to -11.69‰, respectively.

## 5. Discussion

### 5.1. Physical chemistry of stream water

#### 5.1.1. Water temperature

Both $O_2$ and $CO_2$ solubilities are temperature-dependent. The air and water temperature are related in shallow streams. The air temperature during the sampling was steady at around $21^oC$ from 11:00 to 12:00. After 12:00, the air temperature increased 2 ℃ from $21\ ^oC$ to $23^oC$ in one hour and water temperature increased 1.1 ℃ from $18.8^oC$ to $19.9^oC$ within the same time period. Thus, the water temperature increase coincides with the atmospheric temperature increase, and is probably due to solar heating of the shallow stream (20-30 cm deep).

### 5.1.2. pH

The pH ranged from 7.1 to 7.4 from upstream site to downstream site. The water temperature difference (1.1 $^{o}$C) was not enough to result in a change of 0.3 pH units. The relatively high alkalinity (average 383 mg/L) in the streams means that the pH is regulated by the $CO_2$ levels in the water (Neal et al., 2002), i.e., as the $pCO_2$ increases, pH decreases. The $pCO_2$ for the downstream is the lowest, thus, pH is the highest.

### 5.1.3. DO

Solubility of $O_2$ is temperature-dependent: higher water temperature lowers gas solubility. At the sampled sites, the highest DO and DO% was 6.1 mg/L and 65% at 13:00 when stream temperature was also the highest (19.9 $^{o}$C). We propose that aquatic photosynthesis producing $O_2$ was greater than the temperature effect that should have reduced the DO at the downstream location. Nevertheless, the highest DO was still lower than water equilibrated with atmospheric $O_2$ (~9 mg/L at 20$^{o}$C). This suggests that aquatic photosynthesis was active but not active enough to produce more oxygen in the stream than is provided by the groundwater baseflow or consumed by respiration, a conclusion corroborated by the observation of the scarcity of aquatic plants living in the stream.

## 5.2. $CO_2$ outgassing

Streamwater tends to be supersaturated with $CO_2$, that is, out of equilibrium with atmosphere (Butman and Raymond, 2011). The atmospheric $CO_2$ mixing ratio was around 394 ppmv at the time of sampling. $CO_2$ measured in the floating chamber at all three sites ranged from 404 ppmv to 508 ppmv and averaged 454 ppmv (fig. 2.4). This is about 15% higher than the atmospheric $CO_2$ value, indicating $CO_2$ outgassing. The intercepts of the lines reflect the

initial $CO_2$ concentration on the water surface. The downstream intercept is the largest, followed by midstream and upstream. Thus, outgassing is interpreted to be greatest at the downstream site. Moreover, the average chamber $CO_2$ concentrations of upstream and midstream sites were similar (434 ppmv vs 437 ppmv), while downstream site $CO_2$ concentration averaged at 491 ppmv.

$\delta^{13}C_{DIC}$ in the stream can be controlled by the $CO_2$ degassing. $CO_2$ outgassing will cause an enrichment of $\delta^{13}C_{DIC}$ in the residual DIC and a depletion in the $CO_2$ that outgasses. One study documented shifts of $\delta^{13}C_{DIC}$ of up to 5‰ as a result of $CO_2$ degassing at carbonate-hosted springs (Michaelis et al., 1985). In the current study, stream-water $\delta^{13}C_{DIC}$ values were similar at the upstream and midstream sites (-9.46‰ vs -9.50‰) (Table 2.1), while the downstream site stream-water $\delta^{13}C_{DIC}$ (-9.19‰) was heavier. The difference in $\delta^{13}C_{CO2}$ for the upstream and midstream sites was -0.5 and -0.3‰ over the 3.6- and 2.6-minute measuring period (fig. 2.5). This contrasts with the downstream sampling site, where the $\delta^{13}C_{DIC}$ changed by about -1.2‰ over a measurement period of 2.9 minutes. The isotope results corroborate the conclusion that $CO_2$ outgassing at the downstream is greater than the upstream and midstream sites and $\delta^{13}C_{DIC}$ is controlled by $CO_2$ outgassing.

We also used our calculated $pCO_2$ from PHREEQC and gas transfer coefficient ($k_{600}$=0.5 m/d) for small wind-sheltered lakes from Cole et al. (2010) to derive fluxes (Table 2. 4b) for comparison. Our estimated fluxes (Table 2.4a) are 0.5 to 5 times lower than fluxes calculated using the lake $k_{600}$ value (Table 2.4b). This suggests that using the lake gas transfer coefficient for a shallow stream is not appropriate.

### 5.3. Sources of DIC

Kings Creek is an intermittent stream. Continuous flow normally occurs only in the spring season (Mast and Turk, 1999). Under natural conditions, DIC directly coming from soil $CO_2$ can be neglected during carbonate weathering (Dreybrodt, 1988). Therefore, the initial DIC of the stream water was assumed to be from the groundwater input.

Potential sources of DIC in groundwater include downward movement of dissolved $CO_2$ from the soil (Kessler and Harvey, 2001), gas diffusion (Appelo and Postma, 2005), leakage from underlying aquifers, deep $CO_2$ invasion through gas vents (Chiodini et al., 1999), dissolution of carbonate rocks and oxidation of organic matter (Keller and Bacon, 1998). According to Tsypin and Macpherson (2012), soil $CO_2$ and limestone dissolution are the two main sources of DIC in groundwater at Konza; and $HCO_3^-$ contributed more than 90% of anions in groundwater at Konza.

### 5.4. Calculation of POC sources from $\delta^{13}C$ of plant, soil and POC samples

Because $\delta^{13}C$ values are quite different in various carbon pools, it is possible to trace the source and evolution of carbon by using the stable carbon isotope ratios (Fritz et al., 1989). POC transported by streams and rivers comprises a complex mixture of allochthonous and autochthonous sources. For most streams and rivers, the allochthonous fraction dominates the POC in amount and isotopic characteristic. The autochthonous fraction, on the other hand, may be overpowering in some clean and slow-moving waters (Ludwig et al., 1996; Gao et al., 2007). Further, when insolation is the strongest, the water temperature is the highest and photosynthetic activity is the most intense. In this study, the water temperature was highest at the downstream site, coincident with the observed facts in Kings Creek that $\delta^{13}C$ of POC shows negative shift from upstream to downstream.

Although allochthonous POC in stream derives from soil and terrestrial plants, it is necessary to delimit the upper and lower limits of allochthonous POC fraction using soil and terrestrial plants $\delta^{13}C$ separately. Calculated allochthonous POC percentage using soil as an end member for the upstream, midstream and downstream sites is about 65%, 35% and 12%, respectively (Table 2.5). However, using terrestrial plants $\delta^{13}C$ as an end member for allochthonous POC resulted in negative values of the calculated autochthonous fraction, which is unrealistic. Therefore, the allochthonous POC portion cannot originate entirely from land plants and at least part of it should come from the soil. Calculated allochthonous POC fraction using the average soil and terrestrial plants $\delta^{13}C$ for the upstream, midstream and downstream sites is about 88%, 61% and 25%, respectively. The fallem tree leaves in Kings Creek lose 90% of their material between 91 to 1439 days (Gray and Dodds, 1998). Based on observations, all the particles on the filter paper were relatively small suggesting the leaf and root particles from land plants might be neglected. Thus, a larger part of the allochthonous POC in the water should be derived from soil.

Calculations based on the $\delta^{13}C$ show that the contribution of groundwater-sourced carbon to autochthonous POC at the upstream, midstream and downstream sites, based on using soil alone or soil plus plants as the allochthonous end member, is 12-35%, 39-65% and 75-88%, respectively. The downstream site showed the highest contribution from groundwater carbon in POC, suggesting the strongest aquatic photosynthetic effect among the three sites. From equation (3), an independent indicator of photosynthesis, DO showed synchronous change with water temperature. When the sunlight was strong at 13:00, water temperature increased, aquatic plants used DIC and the energy from the sunlight to produce $O_2$. Therefore, the DO and DO% were both the highest in the downstream location and alkalinity was the lowest, although the alkalinity change was small.

### 5.5. Implication of estimated C/N of POC samples

Due to low N content of POC samples, it was not possible to calculate the allochthonous and autochthonous fractions using C/N ratio. Here we use equation (6) to estimate the C/N of POC samples from C/N of plant samples, soil samples and the allochthonous and autochthonous fractions obtained from $\delta^{13}C$. The estimated C/N values of POC samples using soil as the allochthonous source for upstream, midstream and downstream samples are 10, 14 and 12, respectively (Table 2.6); the estimated C/N values of POC samples derived from soil and terrestrial plants average (#4 plant excluded) are 15, 16 and 13, respectively. The POC samples represent suspended POC. According to Dodds et al. (2000), the suspended POC at Konza Prairie has a C/N value of 9 (fig. 2.6). Our estimation of C/N for POC using soil as the allochthonous part is close to their measurement, corroborating our finding, above, that soil should dominate the allochthonous POC.

## 6. Conclusions

To understand spatiotemporal differences in hydrochemistry in Kings Creek, unstable parameters (water temperature, pH, DO, SC and Eh) were measured at three locations from upstream to downstream during midday in May. Soil, plants, water samples and $CO_2$ samples were taken at those three sites. Thermal images suggest that groundwater temperature was around 18.3$^{o}$C and fed the stream from the side and bottom of the stream channel. Results show that the pH ranged from 7.1 to 7.4. The temperature of the downstream streamwater was the highest. DO ranged from 4.7mg/L at the upstream site to 6.1mg/L at the downstream site. The higher DO at the downstream site is attributed to a higher rate of aquatic photosynthesis. $CO_2$ degassing was higher at the downstream site than at the upstream and midstream sites. $\delta^{13}C_{DIC}$

was mainly controlled by $CO_2$ outgassing. There was little variation in the other parameters among the three locations.

The aquatic photosynthesis was the strongest at the downstream site. The autochthonous POC fraction at the upstream, midstream and downstream sites was about 12-35%, 39-65% and 75-88%, respectively. However, the overall aquatic photosynthesis at Konza was not strong due to the lack of submerged plants, evidenced by low DO. Estimation of C/N for POC samples at the three sites is 10-15, 14.0-16 and 12-13. This is comparable to previously measured C/N of suspended POC and corroborates the conclusion that soil dominates the allochthonous POC in this portion of Kings Creek.

**References**

Appelo, C.A.J.P., D., 2005. Geochemistry, Groundwater, and Pollution, 2nd ed. Balkema, Rotterdam.

Berner, R. A., 2004. The Phanerozoic Carbon Cycle: $CO_2$ and $O_2$: Oxford University Press, 150.

Billings, S. A., R. W. Buddemeier, D. deB. Richter, K. Van Oost, and G. Bohling, 2010. A simple method for estimating the influence of eroding soil profiles on atmospheric $CO_2$: Global Biogeochemical Cycles 24, GB2001, doi:10.1029/2009GB003560.

Butman, D., Raymond, P. A., 2011. Significant efflux of carbon dioxide from streams and rivers in the United States. Nat. Geosci. 4, 839-842.

Cole, J. J., D. L. Bade, D. Bastviken, M. L. Pace, and M. Van de Bogert., 2010. Multiple approaches to estimating air-water gas exchange in small lakes. Limnol. Oceanogr. Methods 8, 285–293.

Chiodini, G., Frondini, F., Kerrick, D.M., Rogie, J., Parello, F., Peruzzi, L., Zanzari, A.R., 1999. Quantification of deep $CO_2$ fluxes from Central Italy. Examples of carbon balance for regional aquifers and of soil diffuse degassing. Chemical Geology 159, 205-222.

Dodds, W.K., Evans-White, M.A., Gerlanc, N.M., Gray, L., Gudder, D.A., Kemp, M.J., Lopez, A.L., Stagliano, D., Strauss, E.A., Tank, J.L., Whiles, M.R., Wollheim, W.M., 2000. Quantification of the nitrogen cycle in a prairie stream. Ecosystems 3, 574–89.

Downing, J. A., J. J. Cole, J. J. Middelburg, R. G. Striegl, C. M. Duarte, P. Kortelainen, Y. T. Prairie, and K. A. Laube., 2008, Sediment organic carbon burial in agriculturally eutrophic impoundments over the last century, Global Biogeochem. Cycles, 22, GB1018, doi:10.1029/2006GB002854.

Dreybrodt, W., 1988. Processes in karst systems, Springer, Heidelberg.

Farquhar, G.D., O'Leary, M.H., Berry, J.A., 1982. On the relationship between carbon isotope discrimination and the intercellular carbon dioxide concentration in leaves. Aust. J. Plant Physiol. 9, 121–137.

Fritz, P., Fontes, J.C., Frape, S.K., 1989. The isotope geochemistry of carbon in groundwater at stripa. Geochimica et Cosmochimica Acta 53, 1765–1775.

Gao, Q., Tao, Z., Yao, G., Ding, J., Liu, Z., Liu, K., 2007. Elemental and isotopic signatures of particulate organic carbon in the Zengjiang River, southern China. Hydrol. Process., 21, 1318–1327.

Gray, L.J., and Dodds, W.K., 1998. Structure and dynamics of aquatic communities. In: Knapp, A.K., Briggs, J.M., Hartnett, D.C., Collins, S.L. (Eds.), Grassland Dynamics – Long-Term Ecological Research in Tallgrass Prairie. Oxford University Press, New York, pp. 177–192.

Hydrologic Benchmark Network Stations in the West-Central U.S. 1963-95, USGS Circular 1173-C

Johnson, W.C., Willey, K.L, Macpherson, G.L., 2007. Carbon isotope variation in modern soils of the tallgrass prairie: analogues for the interpretation of isotopic records derived from paleosols. Quat. Int. 162, 3–20

Keller, C.K., Bacon, D.H., 1998. Soil respiration and georespiration distinguished by transport analyses of vadose $CO_2$, $^{13}CO_2$, and $^{14}CO_2$. Global Biogeochem. Cycles 12, 361-372.

Kessler, T.J., Harvey, C.F., 2001. The global flux of carbon dioxide into groundwater. Geophys. Res. Lett. 28, 279-282.

Langmuir D., 1971. The geochemistry of some carbonate ground waters in central Pennsylvania. Geochim. Cosmochim. Acta, 35, 1023–1045.

Liu, Z., Dreybrodt, W., and Wang, H., 2010. A new direction in effective accounting for the atmospheric $CO_2$ budget: Considering the combined action of carbonate dissolution, the global water cycle and photosynthetic uptake of DIC by aquatic organisms. Earth-Sci. Rev., 99, 162–172.

Liu Z, Dreybrodt W, Liu H., 2011. Atmospheric $CO_2$ sink: silicate weathering or carbonate weathering? Applied Geochemistry, 26, 292-294.

Ludwig, W., Probst, J. L., Kempe, S.,1996. Predicting the oceanic input of organic carbon by continental erosion. Global Biogeochem. Cy., 10, 23–41.

Macpherson, G. L., Roberts J. A., Blair J. M., Townsend M. A., Fowle D. A., Beisner K. R., 2008. Increasing shallow groundwater $CO_2$ and limestone weathering, Konza Prairie, USA. Geochimica et Cosmochimica Acta, v. 72, i. 23, pp. 5581-5599.

Mast, M.A., and Turk, J.T., 1999. Environmental characteristics and water quality of Hydrologic Benchmark Network stations in the West -Central United States, 1963–95: U.S. Geological Survey Circular 1173–C, 105 p.

Michaelis, J., Usdowski, E., Menschel, G., 1985. Partitioning of $^{13}C$ and $^{12}C$ on the degassing of $CO_2$ and the precipitation of calcite—Rayleigh type fractionation and a kinetic model. Am. J. Sci. 285, 318-327.

Mook, W.G., Tan, F.C., 1991. Stable carbon isotopes in rivers and estuaries. In: Degens, E.T., Kempe, S., Richey, J.E. (Eds.), Biogeochemistry of Major World Rivers. John Wiley, New York, pp. 345–364.

Neal, C., Watts, C., Williams, R.J., Neal, M., Hill, L., Wickham, H., 2002. Diurnal and longer term patterns in carbon dioxide and calcite saturation for the River Kennet, south-eastern England. Sci. Total Environ. 282, pp. 205–231.

Parkhurst, D., L., and Appelo, C., A., J., 1999. User's guide to PHREEQC (Version 2)—a computer program for speciation, batch-reaction, one-dimensional transport, and inverse geochemical calculations.U.S. Geol. Surv. Wat.-Resour. Investigations Report 99-4259, p. 312.

Putnam, J.E., Lacock, D.L, Schneider, D.R., Carlson, M.D., and Dague, B.J., 1996. Water resources data, Kansas, water year 1995: U.S. Geological Survey Water-Data Report KS–95–1488.

Ransom, M.D., Rice, C.W., Todd, T.C., Wehmueller, W.A., 1998. Soils and soil biota. In: Knapp, A.K., Briggs, J.M., Hartnett, D.C., Collins, S.L. (Eds.), Grassland Dynamics – Long-Term Ecological Research in Tallgrass Prairie. Oxford University Press, New York, pp. 48–66

Sun, H.G., Han, J.T., Zhang, S.R., Lu, X.X., 2011. Transformation of dissolved inorganic carbon (DIC) into particulate organic carbon (POC) in the lower Xijiang River, SE China: an isotopic approach. Biogeosciences Discuss. 8, 9471-950.

Tao, F., Liu, C., Li, S., 2009. Source and flux of POC in two subtropical karstic tributaries with contrasting land use practice in the Yangtze River Basin. Applied Geochemistry, 24, 2102–2112.

Tsypin, M., and Macpherson, G.L., 2012. The effect of precipitation events on inorganic carbon in soil and shallow groundwater, Konza Prairie LTER Site, NE Kansas, USA. Applied Geochemistry 27, 2356–2369.

Wood, H. K. and Macpherson, G. L., 2005. Sources of Sr and implications for weathering of limestone under tallgrass prairie, northeastern Kansas. Applied Geochemistry, 20, 2325-2342.

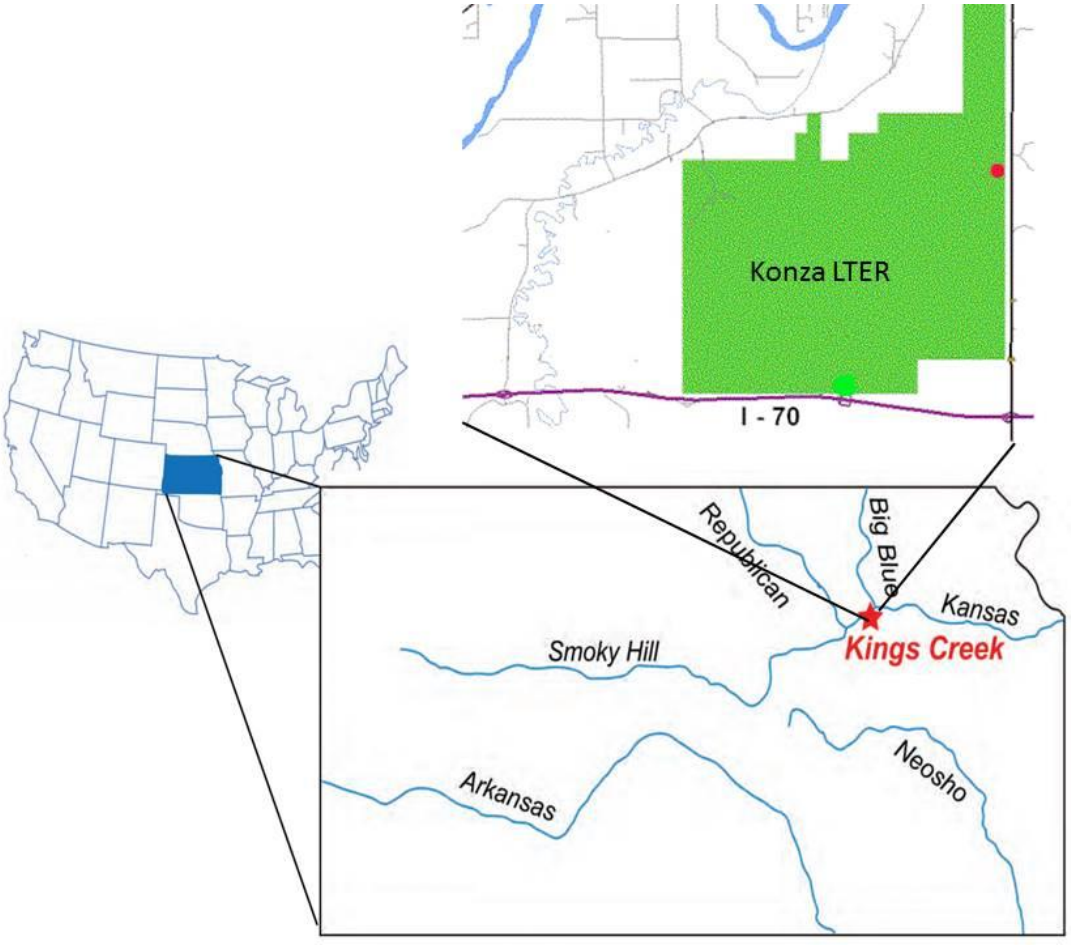


Figure 2.1: Location of Kings Creek and Konza LTER site.

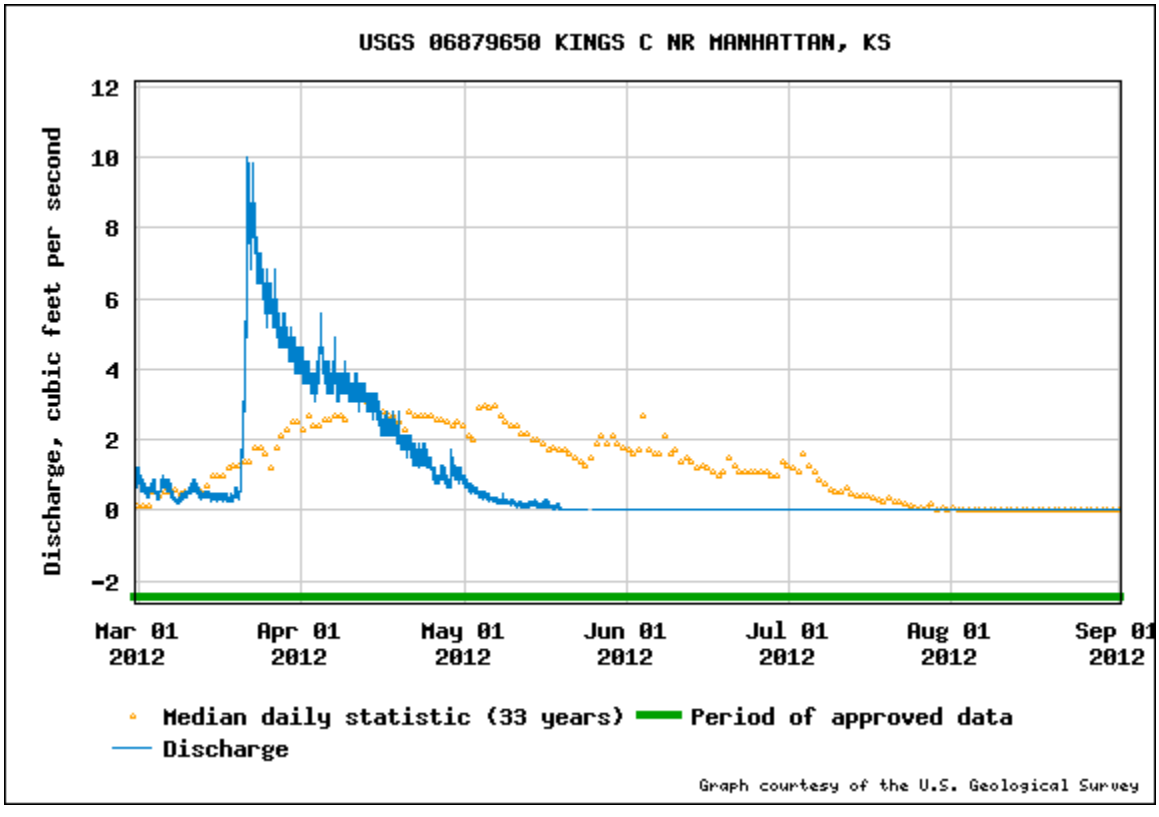


Figure 2.2: USGS discharge graph for Kings Creek from March 2012 to September 2012.

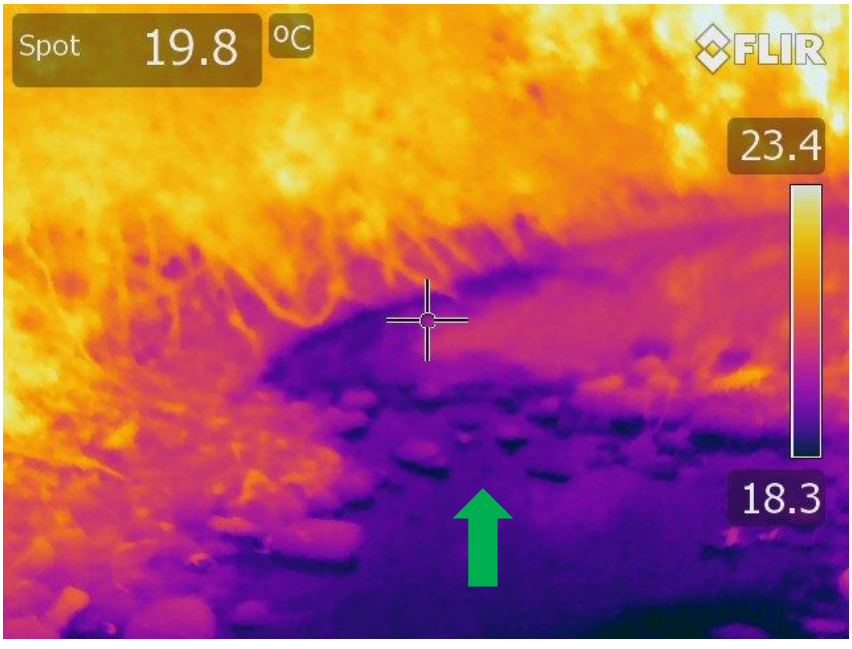


**(a)**

**(b)**

Figure 2.3: Infrared image showing groundwater discharging the stream (a), and visual image of the same location for comparison (b) (Dr. Andrea Brookfield, KGS).

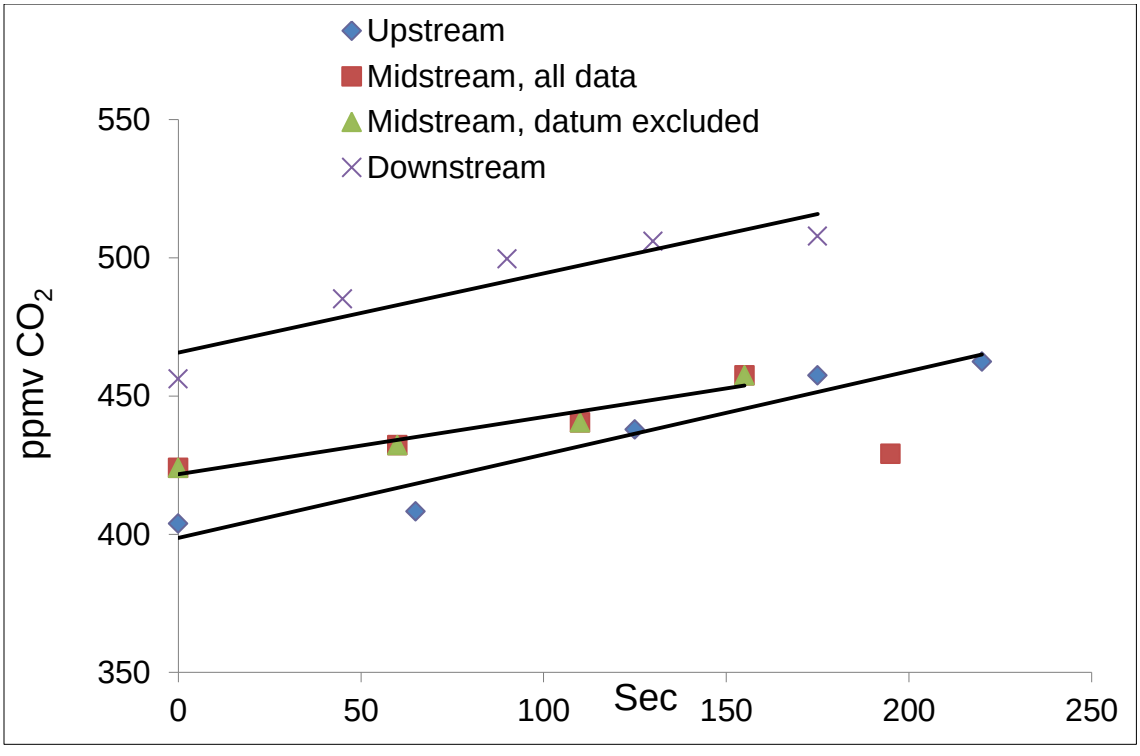


Figure 2.4: Outgassed $CO_2$ concentration vs. time for the upstream, midstream and downstream in the floating chamber (2-sigma error bars are smaller than the symbols).

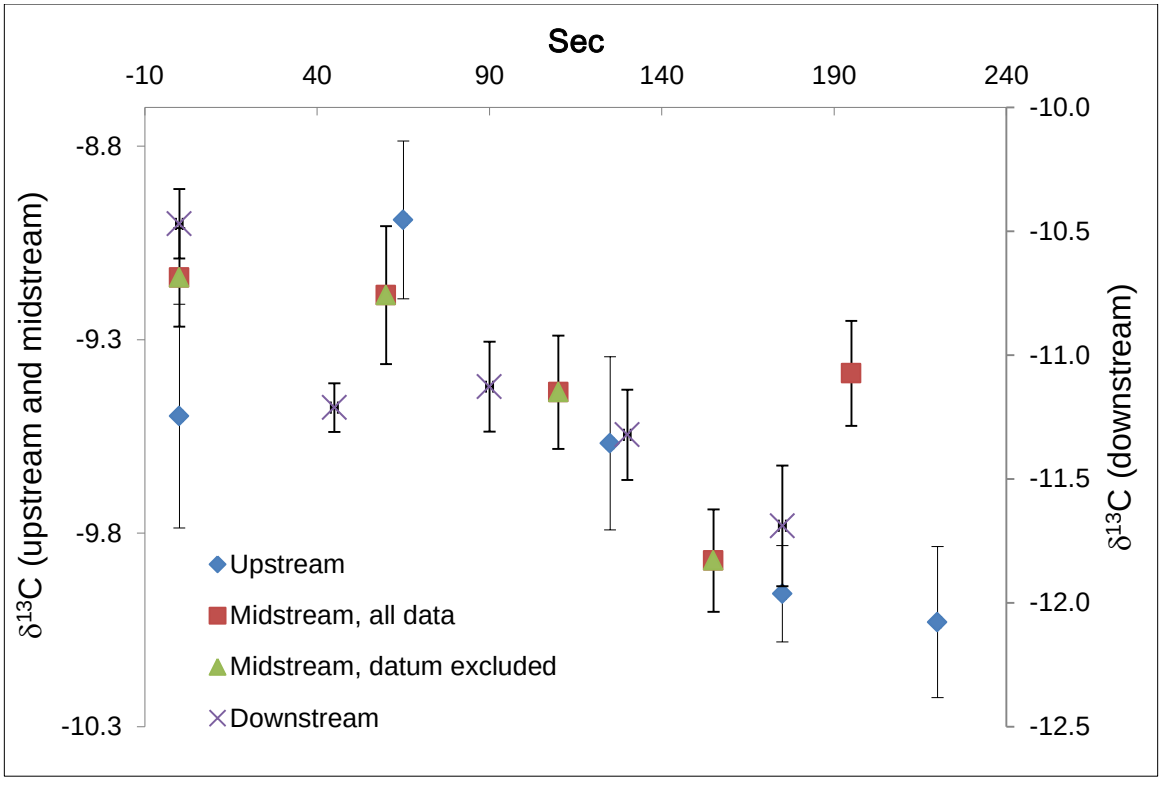


Figure 2.5: $\delta^{13}C$ of $CO_2$ vs. time for the upstream, midstream, and downstream in the floating chamber.

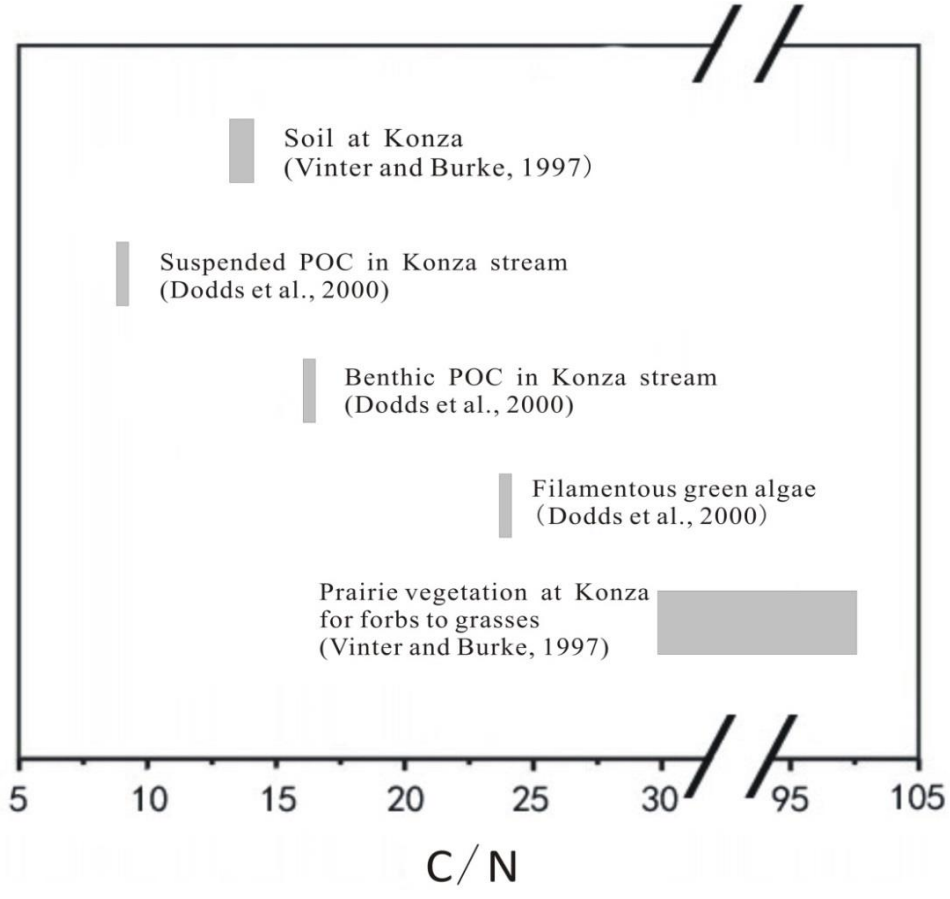


Figure 2.6: C/N values in some reservoirs at Konza Prairie.

Table 2.1: Data for the Konza stream.

| Time | Site | Field pH | T ($^{o}$C) | SC (us/cm) | Eh (mv) | DO (mg/L) | DO% | Alkalinity (mg/L) | Calculated $CO_2$ (ppmv) | $\delta^{13}C_{DIC}$ (‰) |
|---|---|---|---|---|---|---|---|---|---|---|
| 11:20 | Up | 7.3 | 18.8 | 643 | 194 | 4.7 | 51 | 384 | 16800 | $9.46 \pm 0.02$ |
| 12:10 | Mid | 7.1 | 18.9 | 640 | 194 | 4.8 | 51 | 385 | 26800 | $9.50 \pm 0.01$ |
| 13:00 | Down | 7.4 | 19.9 | 637 | 198 | 6.1 | 65 | 380 | 13400 | $9.19 \pm 0.01$ |

Table 2.2: $\delta^{13}C$ and C/N values for the soil, plant and POC samples

| **Identifier** | **$\delta^{13}C$ VPDB(‰)** | **C/N** |
|---|---|---|
| **Soils** | | |
| Upstream | -20.40 | 11.0 |
| Midstream | -18.56 | 10.5 |
| Downstream | -18.66 | 10.6 |
| **Terrestrial plants** | | |
| 1 (*Symphoricarpos orbiculatus*) | -29.50 | 19.4 |
| 2 (*Ulmus*) | -31.08 | 17.7 |
| 3 (C3 unidentified) | -30.13 | 29.8 |
| 4 (*Elymus villosus*) | -31.19 | 82.9 |
| 5 (C3 unidentified) | -30.39 | 23.9 |
| 6 (*Fraxinus pensylvanica*) | -29.12 | 14.6 |
| 7 (C3 unidentified) | -30.72 | 19.3 |
| 8 (*Bromus inermis*) | -26.96 | 22.0 |
| 9 (*Ouercus macrocarpa*) | -29.87 | 18.4 |
| 10 (C3 unidentified) | -28.55 | 23.2 |
| **Aquatic plants** | | |
| Upstream (Green alga) | -35.90 | 9.4 |
| Midstream (*Polygonum*) | -32.71 | 15.9 |
| Downstream (*Veronica*) | -29.96 | 12.4 |
| **POC samples** | | |
| Upstream | -25.86 | |
| Midstream | -27.70 | |
| Downstream | -28.58 | |

Table 2.3: Measured $CO_2$ concentration in the floating chamber.

| **Location** | **Time (sec)** | **$CO_2$ ppmv** |
|---|---|---|
| Upstream | 0 | 404 |
| | 65 | 408 |
| | 125 | 438 |
| | 175 | 457 |
| | 220 | 462 |
| Midstream | 0 | 424 |
| | 60 | 432 |
| | 110 | 440 |
| | 155 | 457 |
| | 195 | 429 |
| Downstream | 0 | 456 |
| | 45 | 485 |
| | 90 | 500 |
| | 130 | 506 |
| | 175 | 508 |

Table 2.4 a: Estimated $CO_2$ flux (F) from $CO_2$ concentration.

| Location | F § (mg/s/m$^2$) | F § (mg/h/m$^2$) | Daily F § (mg/d/m$^2$) |
|---|---|---|---|
| Upstream | 0.090 | 330 | 7800 |
| Midstream | 0.062 | 220 | 5400 |
| Downstream | 0.085 | 310 | 7400 |

§ $Flux(mg/s/m^2) = 0.001963*(dc/dt)*(V/A)*(273.15/T_m)*(P_m/101.325)$ (8)

$Flux(mg/h/m^2) = 7.069*(dc/dt)*(V/A)*(273.15/T_m)*(P_m/101.325)$ (9)

$Flux(mg/d/m^2) = 169.6*(dc/dt)*(V/A)*(273.15/T_m)*(P_m/101.325)$ (10)

dc/dt: increase rate in $CO_2$ partial pressure in the floating chamber; V: chamber volume (5.73 L); A: chamber bottom area (0.035 m$^2$); 273.15: standard temperature in K; $T_m$: the measured temperature of the sampling day in K (22$^o$C+273.15=295.15 K); $P_m$: the measured pressure on the sampling day in kPa (barometric pressure from www.wunderground.com for Manhattan, KS was 29.81 inches Hg, 29.81 * 3.3864 = 100.949 kPa); 101.325: standard pressure in kPa.

Table 2.4 b: Calculated $CO_2$ flux (F) using $k_{600}$.

| Location | F (mg/s/m$^2$) | F (mg/h/m$^2$) | Daily F (mg/d/m$^2$) |
|---|---|---|---|
| Upstream | 0.19 | 670 | 16000 |
| Midstream | 0.30 | 1100 | 26000 |
| Downstream | 0.15 | 530 | 13000 |

$$F=k_{600}*(C_{sur}-C_{eq}) \quad (11)$$

where $k_{600}$ (0.50 m/d) is the piston velocity for a $CO_2$ at $20^oC$, which corresponds to a Schmidt number of 600. $C_{sur}$ and $C_{eq}$ (400 ppmv) are surface water and air-equilibrium concentrations, respectively.

Table 2.5: Calculations of autochthonous and allochthonous fractions in POC

| **Allochthonous POC source** | **Location** | **X(autochthonous fraction, %)** | **1-X(allochthonous fraction, %)** |
|---|---|---|---|
| Soil | Upstream | 35% | 65% |
| | Midstream | 65% | 35% |
| | Downstream | 88% | 12% |
| Terrestrial plants | Upstream | -63% | 163% |
| | Midstream | -70% | 170% |
| | Downstream | -572% | 672% |
| Soil and terrestrial plant average | Upstream | 12% | 88% |
| | Midstream | 39% | 61% |
| | Downstream | 75% | 25% |

Table 2.6: Estimated C/N of POC samples.

| Allochthonous POC source | Location | C/N of POC samples |
|---|---|---|
| Soil | Upstream | 10 |
| | Midstream | 14 |
| | Downstream | 12 |
| Soil and terrestrial plant average | Upstream | 15 |
| | Midstream | 16 |
| | Downstream | 13 |

# CHAPTER 3. DIEL GEOCHEMICAL VARIATIONS IN A KARST SPRING AND TWO PONDS, MAOLAN KARST EXPERIMENTAL SITE, CHINA

**Chapter summary**

A karst spring and two downstream ponds fed by the spring at the Maolan Karst Experimental Site, Guizhou Province, China, were used to investigate the effect of submerged plants on the $CO_2$ system during a time of spring base flow. Temperature, pH, electrical conductivity (EC) and dissolved oxygen (DO) were recorded at 15 min intervals for a period of 30 h (12:00 29 August -18:00 30 August, 2012). [$Ca^{2+}$], [$HCO_3^-$], $CO_2$ partial pressure ($pCO_2$) and saturation index of calcite ($SI_C$) were estimated from the high-frequency measurements. Water samples were also collected three times a day (early morning, midday and evening) for $\delta^{13}C_{DIC}$ determination. A floating $CO_2$-flux monitoring chamber was used to measure $CO_2$ flux at the three locations. Results show that there was little or no diel variation in the spring water parameters. In the midstream pond with flourishing submerged plants, however, all parameters show distinct diel changes: temperature, pH, DO, SIc, $\delta^{13}C_{DIC}$ increased during the day and decreased at night, while EC, [$HCO_3^-$], [$Ca^{2+}$], and $pCO_2$ behaved in the opposite sense. In addition, maximum DO values (16~23 mg/L) in the midstream pond at daytime were two to three times those of water equilibrated with atmospheric $O_2$, indicating strong aquatic photosynthesis. The proposed photosynthesis is corroborated by the low calculated $pCO_2$ of 20-200 ppmv, which is much less than atmospheric $pCO_2$. In the downstream pond with fewer submerged plants but larger volume, all parameters displayed similar trends to the midstream pond but with much less change, a pattern that we attribute to the lower biomass/water volume ratio. The diel hydrobiogeochemical variations in the two ponds depended essentially on illumination, indicating that photosynthesis and respiration by the submerged plants are the dominant controlling processes. The large loss of DIC between the spring and midstream pond, attributed to biological effects, demonstrates that natural surface water systems may constitute an important sink of carbon (on the order of a few hundred tons of C $km^2$/a) as DIC is transformed

to autochthonous organic matter. The rates of sedimentary deposition and preservation of this organic matter in the ponds, however, require quantification in future work to fully assess the karst processes-related carbon cycle, especially under global climate and land use changes.

## 1. Introduction

Hydrobiogeochemical behavior in karst terrains exhibits marked annual, seasonal, and even diurnal and storm-scale variations (Liu et al., 2004; Liu et al., 2006; Liu et al., 2007; Liu et al., 2008). Thus, an increasing number of studies have focused on the karst critical zone because of its sensitivity to environmental changes and distinctive resource-environmental effects (De Montety et al., 2011; Hayashi et al., 2012; Yang et al., 2012; Zeng et al., 2012).

Surface waters in karst terrains are rich in dissolved inorganic carbon (DIC) and provide a well-defined natural system to study gas exchange between water and atmosphere, calcite deposition, aquatic photosynthesis and respiration (Spiro and Pentecost, 1991). Previous studies have emphasized particular aspects of geochemistry or biology in these waters, but data on the interactions among physical, chemical and biological processes are still lacking. These mutually dependent processes should be discussed together, because consideration of water-rock-gas-organism interaction as a whole is required to understand the spatiotemporal hydrobiogeochemical variations in karst waters (Liu et al., 2010; Yang et al., 2012). Moreover, due to the dynamics and complexity of karst processes, there is still much to be learned about the geochemistry of karst waters, especially diel spatiotemporal variation (Liu et al., 2007; Liu et al., 2008; Yang et al., 2012).

A study of dissolved elemental and carbon isotopic composition in the major karst springs at the Maolan Karst Experimental Site, SW China (Maolan) has provided useful information about the characteristics of spring water. Because different sources of dissolved inorganic carbon (DIC) have different isotopic compositions, $\delta^{13}C_{DIC}$ is a direct reflection of the physical, chemical and biological processes in the water (Han et al., 2010). Identifying the transformation of DIC to organic carbon (OC) as evidenced by changes in $CO_2$, $O_2$, DIC, pH,$\delta^{13}C_{DIC}$ and estimating this contribution are the purposes of this study.

Here we report on an investigation of an epikarst spring (Liu et al., 2007) and its two downstream ponds at Maolan. We have obtained high time-resolution monitoring records of the physical-chemical parameters for about a 30-hour period (12:00 29 August -18:00 30 August, 2012). We also report selected $\delta^{13}C_{DIC}$ from the site. This research focuses on the physical chemistry of karst water and the evolution of $\delta^{13}C_{DIC}$ influenced by major natural processes. The aim of this study is to understand diurnal hydrobiogeochemical variations in a typical karst spring and its two downstream ponds under summer, sunny and base flow conditions. These conditions represent the time of most intensive biological activity. The results reveal spatiotemporal differences and their underlying mechanisms, which have implications for assessing karst processes as related to the global carbon cycle (Liu et al., 2010).

## 2. Study area

The Maolan Karst Experimental Site in China (Maolan; fig. 3.1) is well known for its dense virgin evergreen forests growing on cone karst, and is listed by UNESCO as a world heritage site (Libo Karst, one of the three clusters of South China Karst, whc.unesco.org). Annual rainfall in areas with virgin forest is about 1750 mm, about 80% of which falls in the monsoon season from April to September, July and August being the months with highest average precipitation (Zhou, 1987). Annual rainfall is 400 mm less in surrounding deforested areas due to absence of the forest microclimatic effect (Zhou, 1987). The mean annual air temperature at Maolan is about 17 ℃, with hot summers (June–August) and cold winters (December–February). The bedrock is mostly dolomitic limestone of Middle to Lower Carboniferous age (Liu et al., 2007; Jiang et al., 2008).

The sampled spring is a typical Ca-$HCO_3$ type epikarst spring (here termed ‘Maolan spring’) with flow rate of 0.05–30 L/s (Liu et al., 2007). It is at the base of a cone karst slope

covered by virgin karst forest. There is no net deposition of tufa at the spring and the calcite saturation index of the water there is near zero (Liu et al., 2007). Fig. 3.2 gives an oblique perspective of the spring and the receiving ponds with different amounts of submerged plants (chiefly *Charophyta*). The spring and two ponds have been modified by the addition of weirs to control outflow. The spring weir was built in 2002 for long-term monitoring of water stage and hydrogeochemistry (Liu et al., 2007), and the weirs for the two ponds were built in 2004 by the local population for freshwater fish farming; fishing was abandoned in 2011.

The spring discharge was 1.2 L/s and almost stable during the study period, and the surface areas of midstream and downstream ponds were 280 $m^2$ and 1300 $m^2$ respectively. The midstream pond volume was smaller (60 $m^3$) than the downstream pond volume (1300 $m^3$). The distances from the spring orifice sampling site to the midstream pond sampling site was 38 m, and the distance between the midstream and downstream pond sampling sites was 29 m.

## 3. Methods

### 3.1. Field monitoring and sampling

The field study was conducted on 29-30 August 2012 under sunny weather during the wet season. Two WTW® (Wissenschaftlich-Technische-Werkstaetten) Technology MultiLine® 350i's and one SEBA® multi-parameter data logger (Qualilog-16®) were programmed to collect continuous readings of pH, water temperature, dissolved oxygen (DO), and electrical conductivity (EC, 25$^oC$) at 15 min interval for 30 hours (12:00 29 August-18:00 30 August, 2012). The meters were calibrated prior to deployment using pH (4, 7 and 10), EC (1412 μs/cm), and DO (0% and 100%) standards. One WTW-350i® was located at the spring orifice to characterize discharging groundwater. The Qualilog-16® monitored conditions at the midstream

pond and the second WTW-350i® monitored the downstream pond. The resolutions on pH, DO, EC and temp. are 0.01, 0.01 mg/L, 1 μs /cm and 0.01$^{o}$C, respectively.

Water samples for $\delta^{13}C_{DIC}$ were collected three times (midday 29 August; evening 29 August; morning 30 August) at the three sites. The sampling site for the Maolan spring $\delta^{13}C_{DIC}$ differed from the location of the multi-parameter meter: the meter was put in the orifice measuring groundwater conditions just before emergence into the spring pool, whereas the $\delta^{13}C_{DIC}$ samples were collected in the spring pool, after some equilibration with surface conditions. The $\delta^{13}C_{DIC}$ samples were collected in pre-cleaned 30 mL glass vials, with no air space. One drop of saturated $HgCl_2$ solution in each sample served to prevent microbial activity and all samples were kept at temperatures below 4$^{o}$C until analysis.

A floating $CO_2$-flux monitoring chamber (14 L volume with diameter of 40 cm, and surface area of 0.126 m$^2$) was placed on the surface of the waters to determine $CO_2$ efflux from the three sites. $CO_2$ flux was evaluated three times (midday 29 August; evening 29 August; morning 30 August) at each location by collecting five floating-chamber gas samples at 2-min intervals. The $CO_2$ concentration of the samples was measured by gas chromatography (Agilent-7890®) with a resolution of 0.01 ppmv.

### 3.2. Estimating $CO_2$ partial pressure and the calcite saturation index

We attribute EC fluctuations in the spring and ponds to $Ca^{2+}$ and $HCO_3^-$ variations induced by calcite precipitation or dissolution because other dissolved components are not involved in dissolution or precipitation reactions, no rainfall occurred during the sampling interval and evaporation is unlikely because of the high humidity (83% annually, www.163gz.com) of Maolan. $Ca^{2+}$, $Mg^{+2}$ and $HCO_3^-$ were previously correlated with EC at this

site (Liu et al., 2007). The regressions were used to estimate concentrations of $Ca^{2+}$ and $HCO_3^-$ for further calculations, below. The relationships are:

$$[Ca^{2+}] = 0.15\ EC - 0.78,\ r^2 = 0.94, \quad (1)$$

$$[Mg^{2+}] = 0.04\ EC + 0.22,\ r^2 = 0.77, \quad (2)$$

$$[HCO_3^-] = 0.63\ EC - 4.70,\ r^2 = 0.99, \quad (3)$$

where brackets denote concentrations in mg/L and EC is electric conductivity in μS/cm at 25°C (Liu et al., 2007).

Water temperature, pH, estimated $Ca^{2+}$ and $HCO_3^-$, with mean monthly values of $K^+$, $Na^+$, $Mg^{2+}$, $Cl^-$ and $SO_4^{2-}$ (resolutions are 0.01 mg/L) (Liu et al., 2007), were speciated using PHREEQC (Parkhurst and Appelo, 1999) to calculate $CO_2$ partial pressure ($pCO_2$) and the calcite saturation index (SIc) for each record.

### 3.3. Determining DIC and $\delta^{13}C_{DIC}$

The pH of the water in the study ranged from 7.20 to 9.63. At pH 9.6, $HCO_3^-$ and $CO_3^{2-}$ are 84% and 16% of the DIC, respectively. At pH 9, $HCO_3^-$ and $CO_3^{2-}$ constitute 96% and 4% of the DIC, respectively. However, only four pH points for the midstream pond have values higher than 9.5. Thus, calculated $HCO_3^-$ is used as an approximation of DIC for this study.

$\delta^{13}C$ was analyzed on a MAT-252 mass spectrometer with dual inlet. The results are reported relative to the V-PDB standard with an uncertainty less than +/- 0.03‰ (Sun et al., 2011).

## 4. Results

### 4.1. Diel variations in physical chemistry and $\delta^{13}C_{DIC}$

Fig. 3.3 shows the diel variations of the physical chemistry of the Maolan spring and ponds during the study of 29-30 August 2012. Each location is discussed separately, below.

#### 4.1.1. Maolan spring

The pH values of the spring water ranged from 7.11 to 7.28, averaging 7.21. Except for fluctuations of DO (coefficient of variation, CV=4%) and $pCO_2$ (CV=6%; Table 3.1), there was almost no diel change in all of the other physical and chemical parameters at the spring (CV<1.0%, Table 3.1, fig. 3.3). $\delta^{13}C_{DIC}$ of Maolan spring was lowest in the sample collected in the morning and highest at midday (fig. 3.4).

#### 4.1.2. Midstream pond

All parameters in the midstream pond showed distinct changes over the sampling period (fig. 3.3, Table 3.1). Temperature, pH, DO, SIc and $\delta^{13}C_{DIC}$ increased during the day and decreased at night, while EC, $HCO_3^-$, $Ca^{2+}$, and $pCO_2$ decreased in the daytime and increased at the night (figs. 3.3 and 3.4).

Water temperature in the midstream pond ranged from 24.2$^oC$ at 8:00 and 31.8$^oC$ at 16:00 in response to insolation; the mean value was 27.7$^oC$ (fig. 3.3, Table 3.1). Correspondingly, pH, DO, SIc and $\delta^{13}C_{DIC}$ of the waters increased during the day and peaked at 9.62, 23.49 mg/L, 1.62, and -8.4‰, respectively, about an hour or two after temperature was the highest. These parameters gradually declined during the night to reach lowest values (7.47, 0.05 mg/L, 0.03, and -12.3‰, respectively) in the early morning before the sun rose. EC, $HCO_3^-$, $Ca^{2+}$ and $pCO_2$ displayed the reverse of this behavior; EC, estimated $HCO_3^-$, estimated $Ca^{2+}$ and $pCO_2$

continuously decreasing during the day to a minima (249 μs/cm, 152 mg/L, 37 mg/L, and 20 ppmv, respectively) around 18:00, then gradually increased to a maxima (335 μs/cm, 206 mg/L, 50 mg/L, and 6750 ppmv, respectively) in the early morning.

### 4.1.3. Downstream pond

All of the parameters in the downstream pond followed patterns similar to those in the midstream pond from morning to midday but at lower amplitude (fig. 3.3, Table 3.1). Water temperature varied from 26.7$^{o}$C to 30.5$^{o}$C with an average of 28.6$^{o}$C, reaching its minimum at about 8:00 and peak at around 16:00. Similarly, EC, estimated $HCO_3^-$, estimated $Ca^{2+}$ and $pCO_2$ decreased from 301 μS/cm, 185 mg/L, 44 mg/L and 1430 ppmv respectively at 8:00 to 280 μS/cm, 172 mg/L, 41 mg/L and 660 ppmv at around an hour or two after temperature peaked (fig. 3.3, Table 3.1). pH, DO, and SIc of the water increased from 8.12, 6.95 mg/L, and 0.66 respectively at 8:00 to 8.43, 11.5 mg/L, and 0.93 at about one or two hours after maximum temperature.

## 4.2. $CO_2$ flux

### 4.2.1. Maolan spring

Fig. 5a, Table 3.2 and Table 3.3 show that $CO_2$ degassing in the spring pool was the weakest during midday and the most intense in the evening. In the morning, $CO_2$ increased from 504 ppmv to 602 ppmv after 8 minutes, with an efflux of 2500 mg/d/m$^2$. During midday, initial $CO_2$ concentration was 382 ppmv and gradually increased to 416 ppmv after 8 minutes, with an efflux of 1400 mg/d/m$^2$. In the evening, the starting $CO_2$ concentration in the chamber was 566 ppmv and increased to 660 ppmv over the measurement period of 8 minutes, with an efflux of 3100 mg/d/m$^2$.

### 4.2.2. Midstream pond

$CO_2$ concentration ranged from 517 ppmv to 544 ppmv after 6 minutes and 491 ppmv to 518 ppmv after 8 minutes in the morning and evening samplings, respectively, (fig. 3.5b), with both effluxes of 1100 mg/d/$m^2$ (Table 3.3). During midday, there was no $CO_2$ outgassing. Instead, atmospheric $CO_2$ evidently dissolved into the pond water. $CO_2$ started at 364 ppmv in the chamber then gradually decreased to 273 ppmv after 8 minutes, with an influx of -3600 mg/d/$m^2$.

### 4.2.3. Downstream pond

$CO_2$ concentration was the highest in the morning, varying from 534 ppmv to 551 ppmv in the chamber within 8 minutes, with an efflux of 500 mg/d/$m^2$. In the midday and evening, it increased from 385 to 433 ppmv after 8 minutes and 446 to 470 ppmv after 8 minutes respectively, with effluxes of 960 mg/d/$m^2$ and 560 mg/d/$m^2$, correspondingly (fig. 3.5c, Table 3.3).

## 5. Discussion

### 5.1. Mechanisms for DIC and $\delta^{13}C_{DIC}$ changes in the Maolan spring pool

Atmospheric $CO_2$ has an isotopic composition of $\delta^{13}C$ of -7‰, and the isotopic composition of marine limestone is 0 +/-5‰ (Telmer and Veizer, 1999). Generally speaking, the $\delta^{13}C$ of $CO_2$ derived from respiration of C3 plant roots is similar to the $\delta^{13}C_{CO2}$ from degradation of soil organic matter derived from C3 plants, which is close to -24 ± 2‰ (Cerling et al., 1991; Aucour et al., 1999). According to a recent study in the Maolan spring catchment, $\delta^{13}C_{DIC}$ ranges from -8.1‰ to -16.6‰ with a mean value of -13.4‰ (Han et al., 2010), which encompasses the range in this study of -13.4‰ to -14.3‰, with a mean value of -13.9‰ (fig. 3.4). These $\delta^{13}C$

values are lower than those of karst groundwater measured in city springs in southwest China (Han et al., 2010), the difference attributed to the dense virgin forests in Maolan. Han et al. (2010) also showed that 56 ± 9% of the DIC in the Maolan spring water is from degradation of organic matter in the soil and the remainder from dissolution of carbonate.

In this study, the $\delta^{13}C_{DIC}$ of the Maolan spring pool started at -13.4‰ at 13:30 on 29 August then decreased to -14.0‰ at 19:40, and continued decreasing to -14.3‰ at 7:30 of 30 August. It is unlikely that the diel variation of the $\delta^{13}C_{DIC}$ in the spring pool was caused by the dissolution of calcite or the degradation of soil organic matter for the following reasons. First, the degradation of soil organic matter would be the most intense during midday when the air temperature was the highest, resulting in more $CO_2$ entering the groundwater. This would affect the $\delta^{13}C_{DIC}$ in two ways. On the one hand, lighter $CO_2$ from soil organic matter degradation would cause depletion of the $\delta^{13}C_{DIC}$. On the other hand, higher $CO_2$ could drive calcite dissolution and increase the $\delta^{13}C_{DIC}$ because of the heavier $\delta^{13}C$ of limestone. Because the $\delta^{13}C_{DIC}$ at 13:30 was the highest, organic matter degradation is not likely the main influence on the $\delta^{13}C_{DIC}$. Second, the SIc, $[Ca^{2+}]$ and $[HCO_3^-]$ of the spring were stable and SIc was always slightly below 0 (fig. 3.3), indicating the groundwater was undersaturated with respect to calcite. This suggests that there was little precipitation/dissolution of limestone in the spring. Because the diel variation of the $\delta^{13}C_{DIC}$ in the spring pool is not likely controlled by organic matter degradation or calcite dissolution, it is most likely controlled by the change in $CO_2$ efflux or aquatic photosynthetic uptake of $CO_2$.

$CO_2$ outgassing (efflux) causes an enrichment of $\delta^{13}C_{DIC}$ in the residual DIC. One study documented shifts in $\delta^{13}C_{DIC}$ of up to 5‰ as a result of $CO_2$ outgassing at carbonate springs (Michaelis et al., 1985). According to Fig. 3.5a and Table 3.3, $CO_2$ efflux was the weakest at the midday sampling and most intense in the evening. If $CO_2$ efflux was the primary influence on

$\delta^{13}C_{DIC}$, then $\delta^{13}C_{DIC}$ should be the lightest at midday and the heaviest in the evening, the opposite of what is observed. Therefore, the observed $\delta^{13}C_{DIC}$ pattern is most likely related to the change in aquatic photosynthetic uptake of $CO_2$ by the submerged plants in the spring pool (fig. 3.6), stronger during midday when insolation is high than in the early morning and evening. It should be pointed out that the reason why all the physical and chemical parameters of the spring did not fluctuate was because the WTW350i electrode was placed in the spring orifice, free from any photosynthesis activity and thus reflecting the characteristics of groundwater without any modification from the open surface. However, the water samples for the $\delta^{13}C_{DIC}$ determination and degassed $CO_2$ samples were collected in the spring pool where they were already affected by aquatic photosynthesis (fig. 3.7). Because photosynthesis utilizing $CO_2$ was most intense at noontime and in the evening, $CO_2$ outgassing was the weakest at this time, consistent with our data from the floating chamber.

## 5.2. Mechanisms for diel variations in physical, chemical and isotopic properties of the midstream pond

Physical and chemical parameters of surface water may be controlled by groundwater input, temperature changes, gas exchange between water and atmosphere, aquatic photosynthesis and respiration, and calcite precipitation and dissolution (Spiro and Pentecost, 1991). These are discussed below.

### 5.2.1. Groundwater input

From the data in Fig. 3.3, little or no diurnal variations were observed in the physical-chemical parameters of the Maolan spring: groundwater parameters were stable and

thus the diel changes in physical and chemical properties in the midstream pond were not caused by changes in the groundwater input.

### 5.2.2. Temperature

Solubility of both $O_2$ and $CO_2$ are temperature-dependent with higher solubility when water temperature is low. In the midstream pond, pH and DO increased and $pCO_2$ decreased when water temperature increased during the day, and all trends reversed as temperature decreased at night (fig. 3.7a, 3.7b). Although the pH and $pCO_2$ trends follow the expected trends for temperature control on gas solubility, the DO trend is the opposite of what is expected. This suggests that changes in water temperature might not be the major factor controlling pH, $pCO_2$, and DO in the midstream pond during the study period.

### 5.2.3. Gas exchange between water and atmosphere

Inland streams and rivers tend to be $CO_2$-supersaturated with respect to the atmosphere and thus, are a net source of $CO_2$ to the atmosphere (Butman and Raymond, 2011). Gas exchange between water and air can induce large diurnal variations in DO and $pCO_2$, the major controls of Eh and pH (Hoffer-French and Herman, 1989; Liu et al., 2006; Liu et al., 2008). In this study, $pCO_2$ and DO followed opposite trends in the midstream pond (fig. 3.7c).

$CO_2$ outgassing should be the weakest at midday and highest in the morning in the midstream pond, as inferred from the estimated $pCO_2$ values and measured $CO_2$ concentrations in the floating chamber (fig. 3.5, Table 3.2). $CO_2$ degassing enriches $\delta^{13}C_{DIC}$ in streams (Doctor et al., 2008). The expected highest rate of outgassing in the early morning should have yielded the highest $\delta^{13}C_{DIC}$. Instead, the highest $\delta^{13}C_{DIC}$ was at midday, when the estimated $pCO_2$ was the lowest.

These observations and trends indicate that outgassing may not have been the dominant factor controlling pH, concentrations of DO and $CO_2$, and $\delta^{13}C_{DIC}$ during the study period.

### 5.2.4. Photosynthesis and respiration by submerged plants

Diurnal variations of DO and $pCO_2$ are commonly influenced by aquatic photosynthesis and respiration processes which can be approximated by standard equations (e.g., Liu et al., 2008):

$$6H_2O + 6CO_2 \Rightarrow C_6H_{12}O_6 + 6O_2 \qquad \text{Photosynthesis} \qquad (4)$$

$$C_6H_{12}O_6 + 6O_2 \Rightarrow 6H_2O + 6CO_2 \qquad \text{Respiration} \qquad (5)$$

Measured DO showed synchronous variation with water temperature, and inverse correlation with $pCO_2$ (fig. 3.7), suggesting a link to photosynthesis and respiration. During the day when the rate of photosynthesis exceeded respiration, submerged plants used DIC and the energy from the sunlight to produce organic matter and $O_2$. Fig. 3 shows that when sunlight was strong during the day, water temperature increased until 16:00 and DO increased until 18:00. pH of the water increased as photosynthesis consumed $CO_2$. On the other hand, respiration occurs at all times, consuming $O_2$ and releasing $CO_2$.. Therefore, after 16:00 when water temperature started to decrease, DO and pH decreased by the respiration release of $CO_2$ into the water, with a time lag of one or two hours. During the night, in the absence of photosynthesis, respiration was dominant, and consequently DO and pH fell to their minima and $pCO_2$ peaked (fig. 3.3). The inverse relationship between $pCO_2$ and DO over the study period (fig. 3.7c) suggests that the effect of aquatic biological processes surpassed the temperature effect and outgassing. We suggest biological processes are the main factors dominating pH, concentrations of DO and $CO_2$, and $\delta^{13}C_{DIC}$ in the midstream pond on a daily timescale under climatic conditions similar to those during the study period.

### 5.2.5. Calcite precipitation/ dissolution

The decrease in $Ca^{2+}$ concentration between Maolan spring and the midstream pond (fig. 3.3, Table 3.1) suggests that calcite was being precipitated in the midstream pond. During the daytime, submerged plants utilize $CO_2$ and therefore DIC in the ponds, thereby increasing the pH, and potentially driving calcite precipitation. During the nighttime, with the absence of photosynthesis, submerged plants release $CO_2$ back into the water by respiration, thereby increasing the solubility of calcite, and potentially driving calcite dissolution in the midstream pond. The following equations can express these processes (Liu et al., 2010):

$$Ca^{2+} + 2HCO_3^- \Rightarrow CaCO_3 + X(CO_2 + H_2O) + (1\text{-}X)(CH_2O + O_2) \quad \text{(daytime)} \quad (6)$$

$$CaCO_3 + CO_2 + H_2O \Rightarrow Ca^{2+} + 2HCO_3^- \quad \text{(nighttime)} \quad (7)$$

where X and 1-X are stoichiometric numbers.

When calcite precipitates (which enriches $^{13}C$, with ~2‰ heavier than $HCO_3^-$, Deines et al., 1974) and organic matter forms (which enriches $^{12}C$, with ~15‰ lighter than $HCO_3^-$, Sun et al., 2011) during the day, EC, $Ca^{2+}$ and $HCO_3^-$ concentrations all decrease, causing depletion of $^{12}C$ in the remaining DIC in water (i.e., increase in $\delta^{13}C_{DIC}$). At night, the EC, $Ca^{2+}$, $HCO_3^-$ concentrations increase due to calcite dissolution and $\delta^{13}C_{DIC}$ decreases due to release of light $^{12}CO_2$ into water from respiration. However, EC, $Ca^{2+}$ and $HCO_3^-$ in the midstream pond never exceeded those in Maolan spring (fig. 3.3). Moreover, SIc of the midstream water ranged from 0.03~1.62 which is always at least slightly oversaturated with respect to calcite, indicating no carbonate dissolution. Therefore, carbonate dissolution in the midstream pond is an unlikely mechanism contributing to variations in $\delta^{13}C_{DIC}$ on a daily timescale.

### 5.3. Mechanisms for diel variations in physical, chemical and isotopic properties of the downstream pond

An analysis of the same factors addressed in the midstream pond also applies to the downstream pond. When the sun rose at 8:00, the water temperature started to increase and DO increased rather than decreased. Thus, the DO increase likely resulted from aquatic photosynthesis. $pCO_2$ decreased causing higher pH. The variations of the chemical parameters in the downstream pond were much less than those in the midstream pond, as were variations in $\delta^{13}C_{DIC}$ values. In the downstream pond, however, the $\delta^{13}C_{DIC}$ value lower at midday than in the evening may be explained by the deposition of more calcite at midday, which enriches in $^{13}C$, leaving DIC rich in $^{12}C$ (Deines et al., 1974; Michaelis et al., 1985).

The reduced amplitude of the variations in the downstream pond in comparison with the midstream pond may result from the larger volume in the downstream pond that buffered the system. The depth of the downstream pond water was around 1 m, while the depth of the midstream pond water was less than 0.2 m. With the surface areas of about 1310 $m^2$ and 284 $m^2$, water volumes were estimated to be about 1300 $m^3$ and 60 $m^3$ in the downstream and midstream ponds, respectively. The volume effect was further intensified by the lower biomass (submerged plants) in the downstream pond than in the midstream pond, as indicated by the water color (fig.3.2).

### 5.4. Contribution of aquatic biological effects to the stability and sink of carbon

#### 5.4.1. Transformation of DIC into OC: organic carbon preservation potential

The initial DIC of the midstream pond water was contributed mainly by the Maolan spring and the initial DIC of the downstream pond water was controlled by the midstream pond water input. DIC concentration in the midstream and downstream ponds waters were always

lower than that of the spring water. The average estimated DIC concentration of the spring was 224 mg/L, while the average estimated DIC concentrations of the midstream and downstream ponds were 187 mg/L and 182 mg/L, respectively. The decrease in the DIC concentrations between the spring and the midstream pond, and between the midstream pond and the downstream pond reflects the loss of inorganic carbon. The processes influencing the DIC concentrations in the two ponds were: (1) precipitation and dissolution of calcite, (2) exchanges with atmospheric $CO_2$, and (3) aquatic photosynthetic and respiratory.

Since this loss of DIC will be partly transformed into TOC (Sun et al., 2011) as stated in equation (6), and eventually partly buried as autochthonous organic matter (OC) (Liu et al., 2011, Fig. 3.8), it constitutes a "biological carbon pump" (De La Rocha and Passow, 2007) and increases the organic carbon preservation potential in the ponds. Moreover, if the terrestrial "biological carbon pump" effect is strong enough, as in the case of midstream pond, there is even a $CO_2$ sink directly from the atmosphere to surface waters (fig. 3.5b, Table 3.3) as discussed below in more detail.

### 5.4.2. $CO_2$ influx from atmosphere to water: insight from the floating chamber data in the midstream pond

During 13:00-19:00, the strong aquatic photosynthesis (with high DO concentrations) resulted in $pCO_2$ levels of less than 100 ppmv (Fig. 3.3, Table 3.1). Further, $CO_2$ concentration in the chamber started with 364 ppmv at 14:51 then gradually decreased to 273 ppmv after 8 minutes (fig. 3.5b). The $pCO_2$ in the chamber was lower than that of the atmosphere (around 390 ppmv), suggesting that there was $CO_2$ influx from the atmosphere to water instead of $CO_2$ evasion. This phenomenon in the midstream pond suggests that strong aquatic photosynthesis in terrestrial surface waters might form another important natural carbon sink by drawing $CO_2$

directly from the atmosphere, as occurs in the oceans (Ducklow et al., 2001; Passow and Carlson, 2012).

### 5.4.3. Quantification of daily organic carbon formation in the two ponds

The decrease in DIC between Maolan spring and the ponds results from the joint effects of calcite precipitation, exchanges with atmospheric $CO_2$, and aquatic photosynthesis. We have used the decrease in $Ca^{2+}$ concentrations to predict calcite precipitation (Table 3.1) and the flux of exchanges with atmospheric $CO_2$ (Table 3.3) in the two ponds. The daily organic carbon formation in the two ponds can be estimated as follows:

$$M_{OC}=Q*(DIC_1-DIC_2)/5.080 - Q*(Ca_1-Ca_2)/3.337 - (F/3.664)*A$$

where $M_{OC}$ is mass of organic carbon formed in a day (mg/d); Q is the discharge of the stream (i.e., the discharge of the spring if evaporation is ignored under conditions of high humidity, L/d), $DIC_1$ and $DIC_2$ are the $HCO_3^-$ concentrations at the inlet and outlet of the pond (in mg/L), 5.080 is the $HCO_3^-$—carbon conversion factor, $Ca_1$ and $Ca_2$ are the $Ca^{2+}$ concentrations in mg/L at the inlet and outlet of the pond, respectively, 3.337 is the calcium-carbon conversion factor, (40.08/12.011), F is the $CO_2$ flux from water surface (mg/d/$m^2$), 3.664 is the $CO_2$-carbon conversion factor, and A is the area of pond water surface ($m^2$).

For the midstream pond:

$M_{OC}$=103680*(223.6-186.6)/5.080-103680*(53.5-44.8)/3.337-(-450/3.664)*280

=519000 (mg/d);

For the downstream pond:

$M_{OC}$=103680*(186.6-182)/5.080-103680*(44.8-43.7)/3.337-(670/3.664)*1300

= -178000 (mg/d).

Therefore, the organic carbon sink flux by the submerged plants in the midstream pond is ~1850 mg/d/$m^2$, equivalent to 677 t C/$km^2$/a, which shows the significant role of submerged plants in stabilizing the carbon sink by karst processes (carbonate weathering) (from DIC to TOC) and/or uptake of $CO_2$ directly from the atmosphere.

The organic carbon sink flux in the downstream pond is -137 mg/d/$m^2$, equivalent to -49.9 t C/$km^2$/a, the negative value showing no net organic carbon sink by the few submerged plants in the downstream pond, but, instead, release of $CO_2$ by decomposition of allochthonous organic matter. We assume this organic matter is the legacy of fish farming, ceased ~ 1 year before this study, in the downstream pond.

## 6. Conclusions

Physical and chemical parameters (water temperature, pH, DO, and EC) were monitored at high time-resolution (15 min) over a 30-hour period to investigate the controls on hydrobiogeochemistry at the Maolan Karst Experimental Site, Guizhou province, China. The study site included a karst spring and two downstream ponds with different development of submerged plants, and sampling occurred under wet-season, summer, sunny, base-flow conditions. [$Ca^{2+}$], [$HCO_3^-$], $CO_2$ partial pressure ($pCO_2$) and saturation index of calcite (SIc) were estimated from the high-resolution measurements. Samples for $\delta^{13}C_{DIC}$ were collected three times over the 30-hour period (midday, early evening and early morning) at the three locations. Gas samples collected from a floating chamber were used to calculate $CO_2$ efflux from the three locations.

Results show that there was little or no diel variation in most of the spring physical and chemical parameters. The midstream pond, assumed to have received input only from the spring ~38 meters upgradient, was filled with submerged plants, and all physical and chemical

parameters showed distinct diel changes. The temperature, pH, DO, SIc, $\delta^{13}C_{DIC}$ in the midstream pond increased during the day and decreased at night, while EC, $HCO_3^-$, $Ca^{2+}$, and $pCO_2$ decreased during the day and increased at the night. The maximum DO values (16~23 mg/L) in the midstream pond during the day were twice to three times those expected of water equilibrated with atmospheric $O_2$, suggesting aquatic photosynthesis. The midstream pond had the lowest estimated $pCO_2$ of the three locations, at 20 ppmv, which is much less than the atmospheric $CO_2$ concentration, also suggesting aquatic photosynthesis. In addition, during the midday sampling time, the $CO_2$ flux direction was from the atmosphere into water. The downstream pond had only a few submerged plants. At this location, all of the parameters varied similarly to the midstream pond location, but with much lower amplitude. We suggest this results from the dilution effect because of the lower biomass/water tank ratio. The diel hydrobiogeochemical temporal variations in the two ponds are consistent with results expected from aquatic photosynthesis and respiration.

The large loss of DIC between spring and midstream pond is attributed to biological storage of carbon, demonstrating that natural surface waters may constitute an important carbon sink. Since this loss of DIC is at least partly and likely mostly transformed into TOC, burial as autochthonous organic matter constitutes a "terrestrial biogeochemical carbon pump" (TBCP). Moreover, if the TBCP effect is strong enough, as in the case of midstream pond under optimum photosynthesis conditions, there is a $CO_2$ sink directly from the atmosphere to surface waters.

The distribution and extent of surface waters with strong TBCP is as yet unknown. In addition, sedimentation and preservation rates of autochthonous OC (fig.3.8) in terrestrial surface water is also poorly known, especially under rapid global climate and land use changes occurring recently. This study suggests that an important goal in improving global carbon budgets may include quantifying the importance of the TBCP in terrestrial aquatic settings.

**References**

Aucour, A. M., Sheppard, S. M. F., Guyomar, O., Wattelet, J., 1999. Use of $^{13}C$ to trace origin and cycling of inorganic carbon in the Rhone river system. Chem. Geol. 159, 87–105.

Butman, D., Raymond, P. A., 2011. Significant efflux of carbon dioxide from streams and rivers in the United States. Nat. Geosci. 4, 839-842.

Cerling, T. E., Solomon, D. K., Quade, J., 1991. On the isotopic composition of carbon in soil carbon dioxide. Geochim Cosmochim Acta 55, 3403–3405.

De La Rocha, C. L., Passow, U., 2007. Factors influencing the sinking of POC and the efficiency of the biological carbon pump. Deep Sea Res. 54, 639–658.

De Montety, V., Martin, J.B., Cohen, M.J., Foster, C., Kurz, M.J., 2011. Influence of diel biogeochemical cycles on carbonate equilibrium in a karst river. Chem. Geol. 283, 31-43.

Deines, P., Langmuir, D., Harmon, R. S., 1974. Stable carbon isotope ratios and the existence of a gas phase in the evolution of carbonate ground waters. Geochim. Cosmochim. Acta. 38, 1147-1164.

Doctor, D. H., Kendall, C., Sebestyen, S. D., Shanley, J.B., Ohte, N., Boyer, E.W., 2008. Carbon isotope fractionation of dissolved inorganic carbon (DIC) due to outgassing of carbon dioxide from a headwater stream. Hydrol. Process. 22, 2410-2423.

Ducklow, H. W., Steinberg, D. K., Buesseler, K. O., 2001. Upper ocean carbon export and the biological pump. Oceanography 14, 50-58.

Han, G., Tang, Y., Wu, Q., 2010. Hydrogeochemistry and dissolved inorganic carbon isotopic composition on karst groundwater in Maolan, southwest China. Environ. Earth Sci. 60, 893-899.

Hayashi, M., Vogt, T., Machler, L., Schirmer, M., 2012. Diurnal fluctuations of electrical conductivity in a pre-alpine river: Effects of photosynthesis and groundwater exchange. J. Hydrol. 450, 93-104.

Hoffer-French, K., Herman, J., 1989. Evaluation of hydrological and biological influences on $CO_2$ fluxes from a karst stream. J. Hydrol. 108, 189-212.

Jiang, G., Guo, F., Wu, J., Li, H., Sun, H., 2008. The threshold value of epikarst runoff in forest karst mountain area. Environ. Geol. 55, 87-93.

Liu, Z., Groves, C., Yuan, D., Meiman, J., Jiang, G., He, S., 2004. Hydrochemical variations during flood pulses in the southwest China peak cluster karst: Impacts of $CaCO_3$-$H_2O$-$CO_2$ interactions. Hydrol. Proc. 18, 2423－2437.

Liu, Z., Li, Q., Sun, H., Liao, C., Li, H., Wang, J, Wu, K., 2006. Diurnal variations of hydrochemistry in a travertine-depositing stream at Baishuitai, Yunnan, SW China. Aquat. Geochem. 12, 103-121.

Liu, Z., Li, Q., Sun, H., Wang, J., 2007. Seasonal, diurnal and storm-scale hydrochemical variations of typical epikarst spring in subtropical karst areas of SW China: soil $CO_2$ and dilution effects. J. Hydrol. 337, 207–223.

Liu, Z., Liu, X., Liao, C., 2008. Daytime deposition and nighttime dissolution of calcium carbonate controlled by submerged plants in a karst spring-fed pool: insights from high time-resolution monitoring of physico-chemistry of water. Environ. Geol. 55, 159-1168.

Liu, Z., Dreybrodt, W., Wang, H., 2010. A new direction in effective accounting for the atmospheric $CO_2$ budget: Considering the combined action of carbonate dissolution, the global water cycle and photosynthetic uptake of DIC by aquatic organisms. Earth-Sci. Rev. 99, 162-172.

Liu, Z., Dreybrodt, W., Liu, H., 2011. Atmospheric $CO_2$ sink: silicate weathering or carbonate weathering? Appl. Geochem. 26, 292-294.

Michaelis, J., Usdowski, E., Menschel, G., 1985. Partitioning of $^{13}C$ and $^{12}C$ on the degassing of $CO_2$ and the precipitation of calcite—Rayleigh type fractionation and a kinetic model. Am. J. Sci. 285, 318-327.

Parkhurst, D., L., and Appelo, C., A., J., 1999. User's guide to PHREEQC (Version 2)—a computer program for speciation, batch-reaction, one-dimensional transport, and inverse geochemical calculations.U.S. Geol. Surv. Wat.-Resour. Investigations Report 99-4259, p. 312.

Passow, U., Carlson, C. A., 2012. The biological pump in a high $CO_2$ world. Mar. Ecol. Prog. Ser. 470, 249–271.

Spiro, B., Pentecost, A., 1991. One day in the life of a stream—A diurnal inorganic carbon mass balance for a travertine-depositing stream (Waterfall Beck, Yorkshire). Geomicrobiol. J. 9, 1-11.

Sun, H.G., Han, J.T., Zhang, S.R., Lu, X.X., 2011. Transformation of dissolved inorganic carbon (DIC) into particulate organic carbon (POC) in the lower Xijiang River, SE China: an isotopic approach. Biogeosci. Discus. 8, 9471-9501.

Telmer, K., Veizer, J., 1999. Carbon fluxes, $pCO_2$ and substrate weathering in a large northern river basin, Canada: carbon isotope perspectives. Chem. Geol. 159, 61–86.

Yang, R., Liu, Z., Zeng, C., Zhao, M., 2012. Response of epikarst hydrochemical changes to soil $CO_2$ and weather conditions at Chenqi, Puding, SW China. J. Hydrol. 468-469, 151-158..

Zeng, C., Gremaud, V., Zeng, H., Liu, Z., Goldscheider, N., 2012. Temperature-driven meltwater production and hydrochemical variations at a glaciated alpine karst aquifer: implication for the atmospheric $CO_2$ sink under global warming. Environ. Earth Sci. 65, 2285–2297.

Zhou, Z., 1987. Scientific Survey of the Maolan Karst Forest. Guizhou Peoples' Publishing House, Guiyang.


Figure 3.1: Location of the Maolan karst experimental site and Maolan spring (monitoring site) (modified from Jiang et al., 2008).


Figure 3.2: Maolan spring and the spring-fed midstream pond with flourishing submerged plants and downstream pond with few submerged plants due to use of herbicide by local farmer. The red circles represent the positions of the measuring points where continuous data were acquired. The surrounding vegetation cover is virgin karst forests.

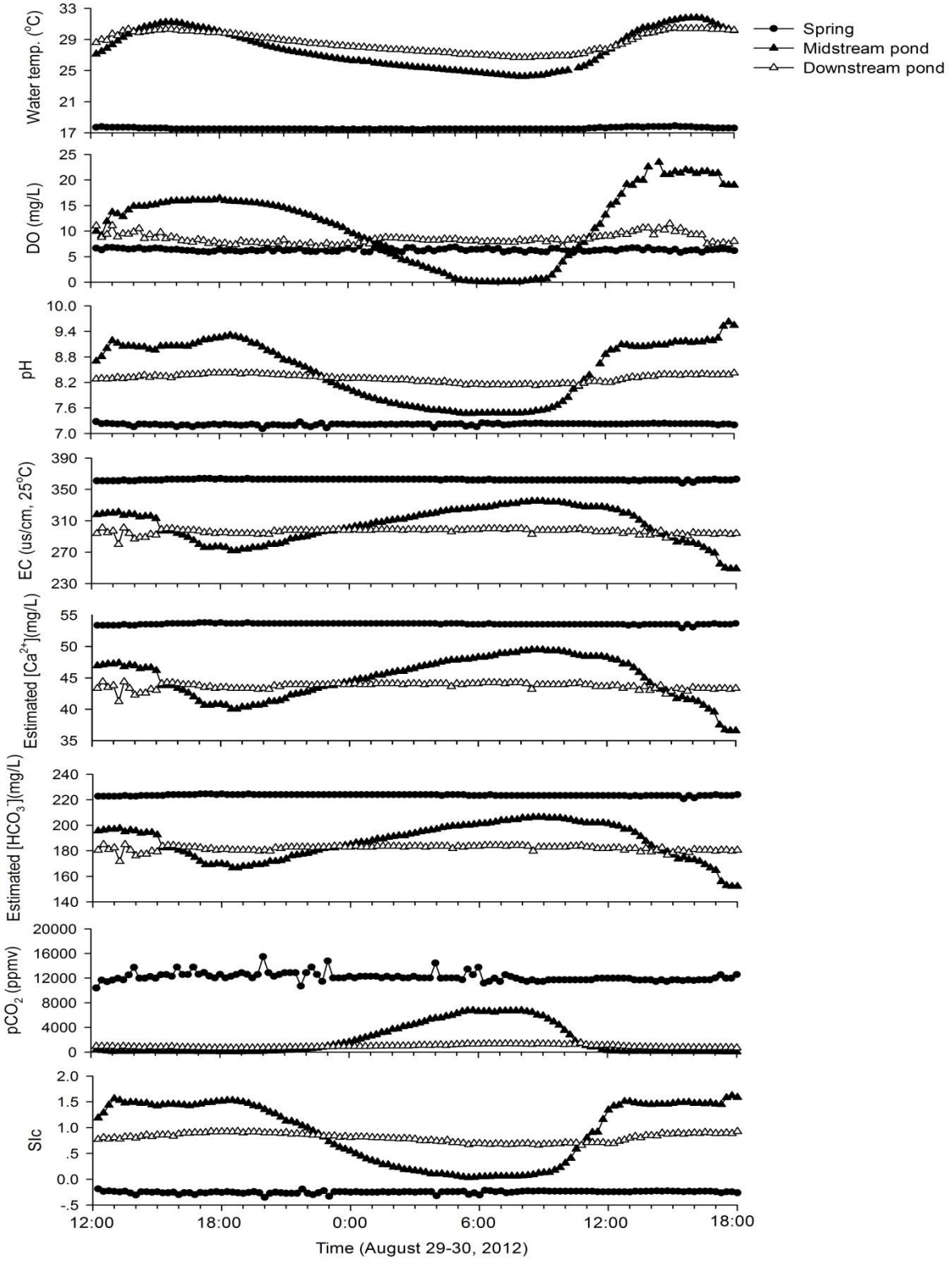


Figure 3.3: The diel variations of the physical-chemical parameters of Maolan spring (orifice) and the midstream and downstream ponds (2-sigma error bars are smaller than the symbols).

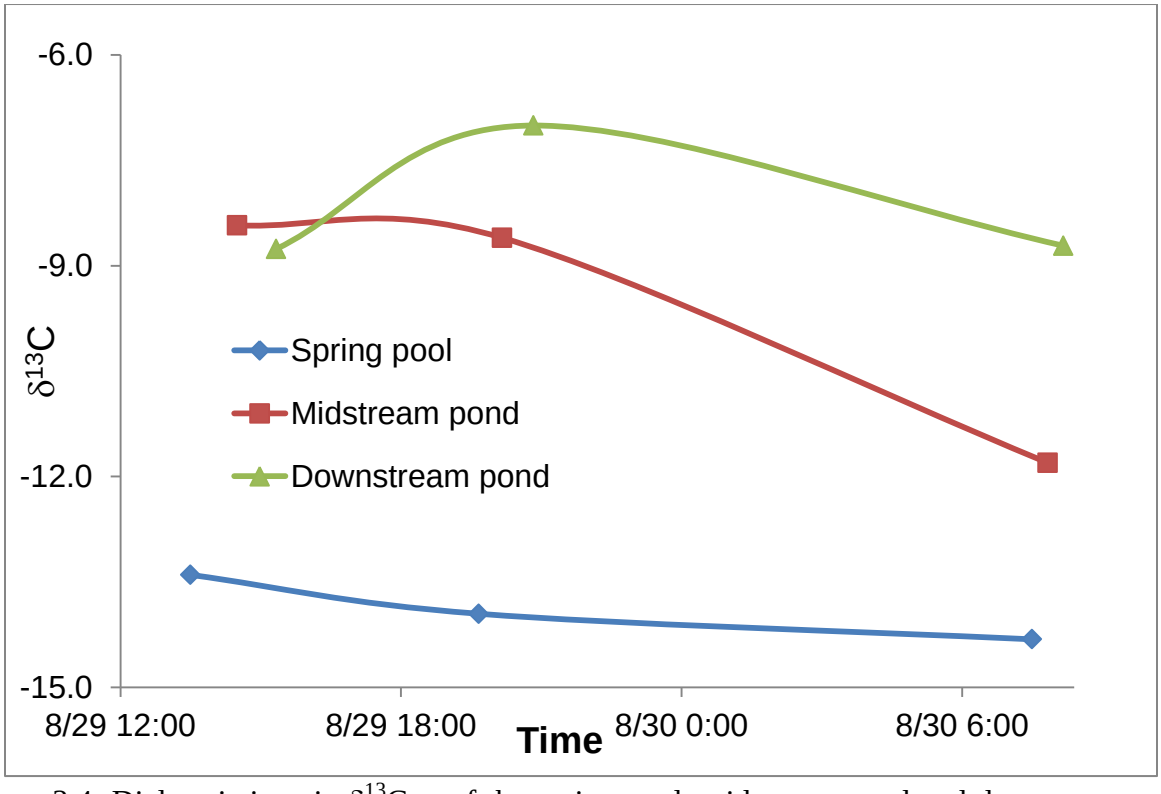


Figure 3.4: Diel variations in $\delta^{13}C_{DIC}$ of the spring pool, midstream pond and downstream pond (2-sigma error bars are smaller than the symbols).

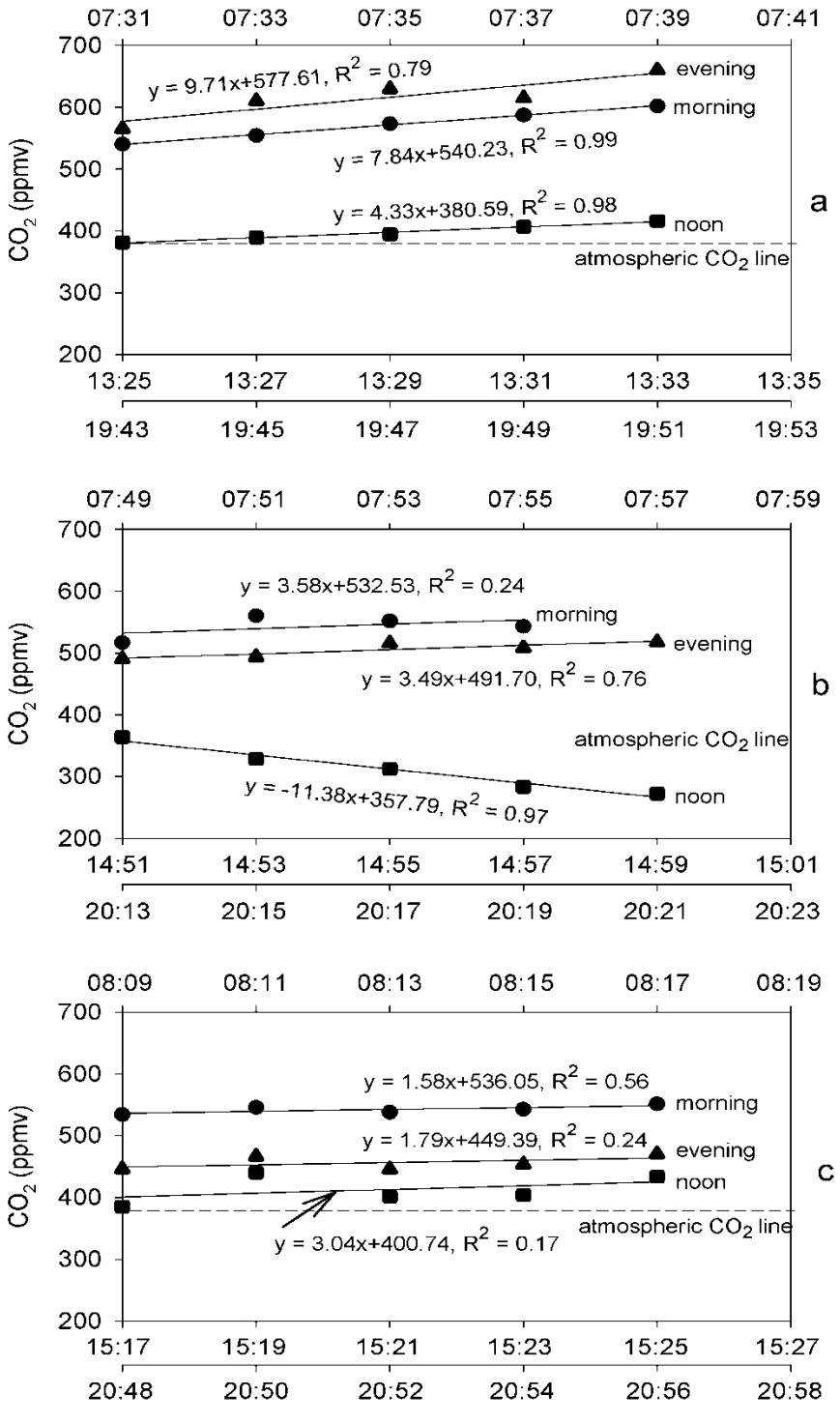


Figure 3.5: $CO_2$ variations in the floating chamber located in the spring pool (a), midstream pond (b) and downstream pond (c) in the early morning, at midday and in the evening (2-sigma error bars are smaller than the symbols).


Figure 3.6: The Maolan spring pool with development of submerged plants.

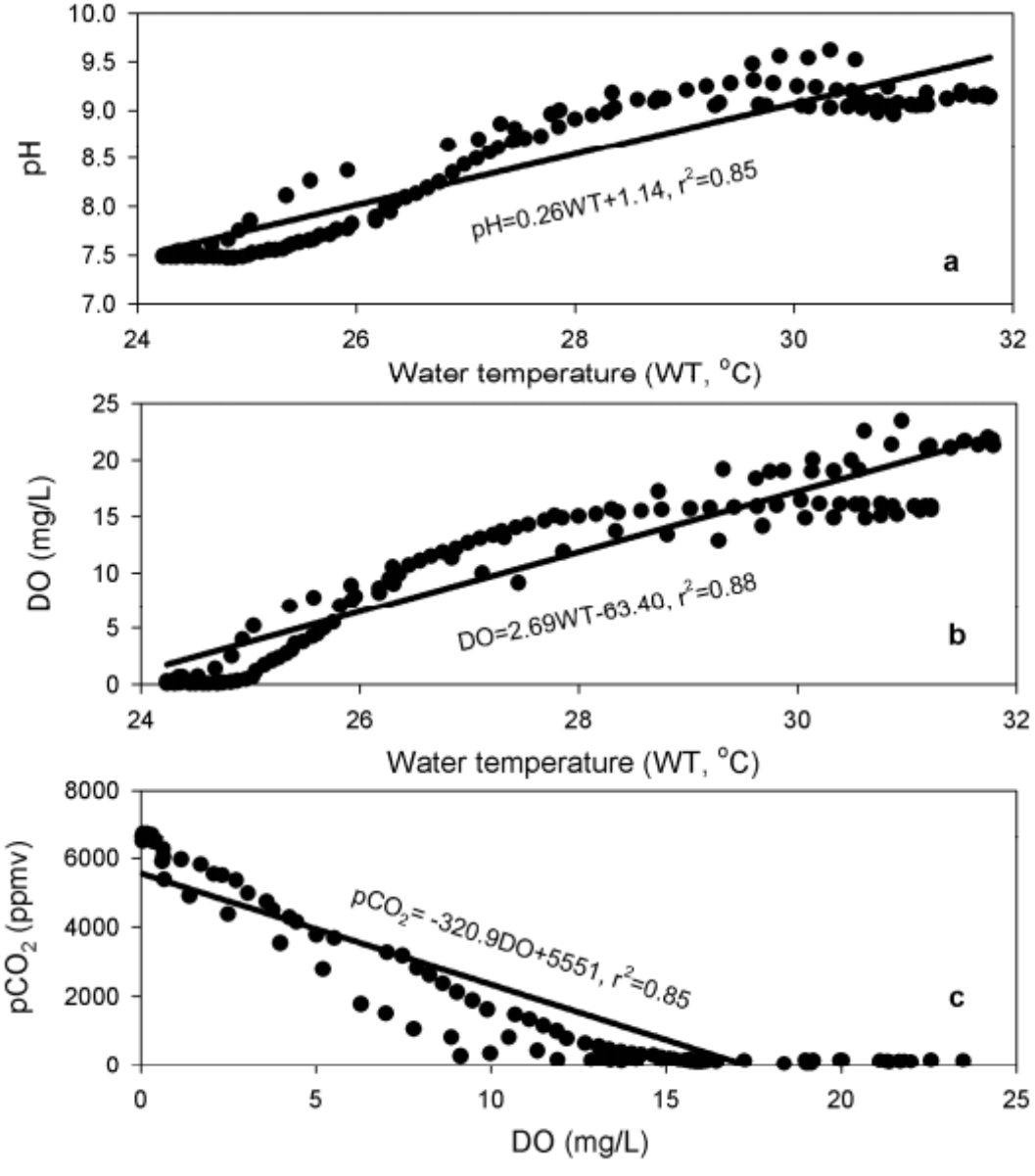


Figure 3.7: Relationship between pH and water temperature (a), between DO and water temperature (b), and between $pCO_2$ and DO (c) in the midstream pond (2-sigma error bars are smaller than the symbols).

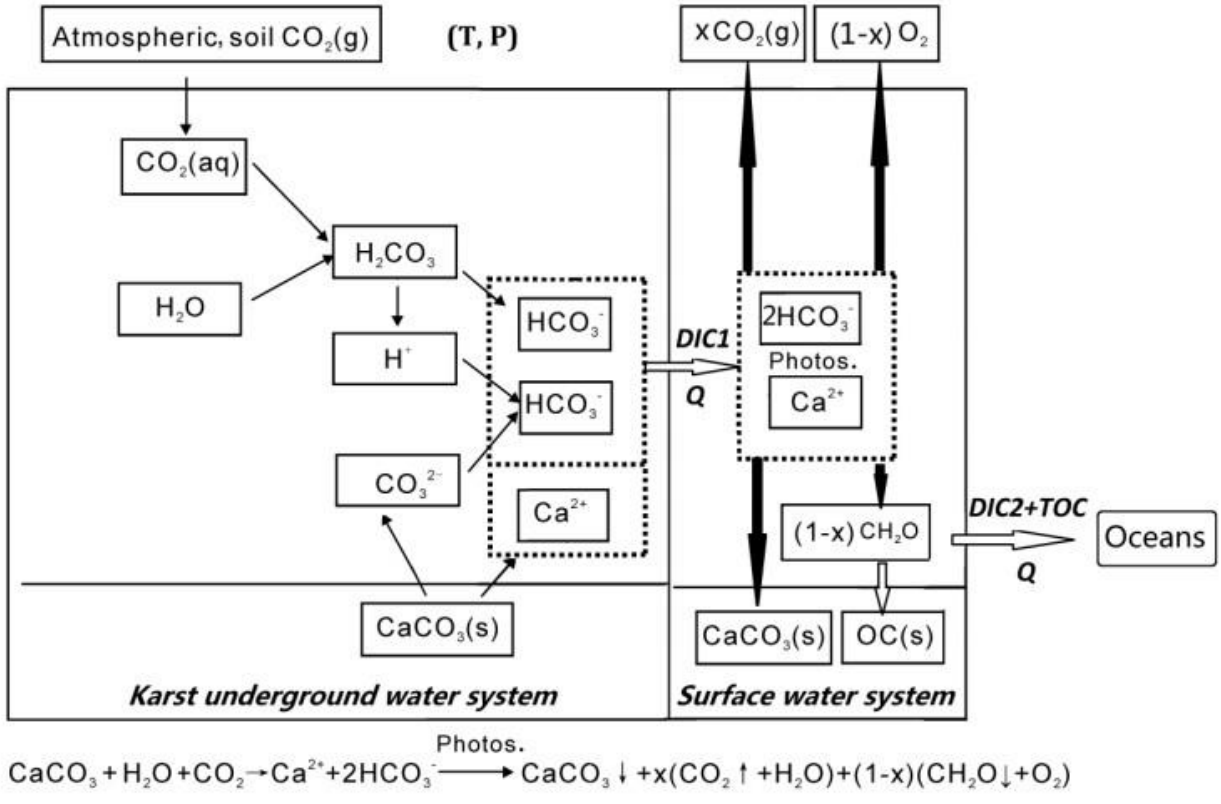


Figure 3.8: Conceptual model of the carbon cycle in karst settings based on water-rock-gas-biota interactions (drawing in reference to Liu et al., 2011).

T, P and Q are the air temperature, precipitation and discharge of a karst catchment area respectively. $DIC_1$ and $DIC_2$ are the concentrations of dissolved inorganic carbon in the karst underground water system and surface water system respectively, and TOC is the concentration of total organic carbon in surface water system transformed from $DIC_1$ by the submerged plants via photosynthesis. OC(s) is the sedimentation of organic carbon.

Note: Unlike the traditional carbonate weathering carbon cycle model, which only considers water-rock-gas interaction (ignoring the organic matter deposition formed by aquatic photosynthetic uptake of DIC), this model helps to answer important questions such as whether carbonate weathering could be a long-term carbon sink, if accompanied by burial of autochthonous organic matter, thus controlling long-term climate change.

Table 3.1: Daily minimum, maximum, mean values of hydrobiogeochemical parameters in Maolan spring and two ponds during August 29-30, 2012

| | | Maolan spring | | | Midstream pond | | | Downstream pond | | |
|---|---|---|---|---|---|---|---|---|---|---|
| Item | Unit | Min. | Max. | Mean (n=120) | Min. | Max. | Mean (n=120) | Min. | Max. | Mean (n=120) |
| Temp. | $^{o}C$ | 17.4 | 17.9 | 17.6 | 24.2 | 31.8 | 27.7 | 26.7 | 30.5 | 28.6 |
| DO | mg/L | 5.79 | 7.05 | 6.34 | 0.05 | 23.49 | 11.31 | 6.95 | 11.46 | 8.46 |
| pH | - | 7.11 | 7.28 | 7.21 | 7.47 | 9.62 | 8.5 | 8.12 | 8.43 | 8.29 |
| EC | μs/cm | 358 | 364 | 362 | 249 | 335 | 304 | 280 | 301 | 296 |
| $Ca^{2+}$ | mg/L | 52.9 | 53.8 | 53.6 | 36.6 | 49.5 | 44.8 | 41.2 | 44.4 | 43.7 |
| $HCO_3^-$ | mg/L | 220.8 | 224.6 | 223.6 | 152.2 | 206.4 | 186.6 | 172 | 185 | 182 |
| $SI_C$ | - | -0.35 | -0.19 | -0.25 | 0.03 | 1.62 | 0.93 | 0.66 | 0.93 | 0.81 |
| $pCO_2$ | ppmv | 10400 | 15500 | 12200 | 20 | 6750 | 1910 | 660 | 1430 | 950 |

Table 3.2: Measured $CO_2$ concentration in the floating chamber.

| **Location** | **Time** | **$CO_2$ ppmv** | | | | |
|---|---|---|---|---|---|---|
| Spring pool | Morning (7:31-7:39) | 540 | 555 | 574 | 588 | 602 |
| | Midday (13:25-13:33) | 382 | 390 | 395 | 407 | 416 |
| | Evening (19:43-19:51) | 566 | 611 | 630 | 615 | 660 |
| Midstream | Morning (7:49-7:55) | 517 | 560 | 552 | 544 | |
| | Midday (14:51-14:59) | 364 | 329 | 312 | 284 | 273 |
| | Evening (20:13-20:21) | 491 | 494 | 516 | 509 | 518 |
| Downstream | Morning (8:09-8:17) | 534 | 546 | 538 | 543 | 551 |
| | Midday (15:17-15:25) | 385 | 440 | 402 | 404 | 434 |
| | Evening (20:48-20:56) | 446 | 467 | 446 | 454 | 470 |

Table 3.3: Estimation of $CO_2$ flux (F) in the floating chamber in Maolan spring pool and the spring-fed two ponds in the morning, midday and evening.

| **Location** | **time** | **F ($mg/s/m^2$)** | **F ($mg/h/m^2$)** | **Daily F ($mg/d/m^2$)** |
|---|---|---|---|---|
| Spring pool | Morning(7:31-7:39) | 0.029 | 100 | 2500 |
| | Midday(13:25-13:33) | 0.016 | 57 | 1400 |
| | Evening(19:43-19:51) | 0.035 | 130 | 3100 |
| Midstream pond | Morning(7:49-7:55) | 0.013 | 47 | -1100 |
| | Midday(14:51-14:59) | -0.042 | -150 | -3600 |
| | Evening(20:13-20:21) | 0.0123 | 46 | 1100 |
| Downstream pond | Morning(8:09-8:17) | 0.0058 | 21 | 500 |
| | Midday(15:17-15:25) | 0.011 | 40 | 960 |
| | Evening(20:48-20:56) | 0.0065 | 24 | 560 |

# APPENDICIES

## Appendix A. Methods for Konza May sampling

### Sampling detail on 25 May

At around 11:20 am we were at the upstream site. a) We measured and recorded unstable parameters in this order of pH, EC, DO, Eh, temperature. Before measurements, we calibrated Fisher Accumet 1003 probe with pH buffer 4, 7; calibrate EC with solution (1409 uS), then collected water sample in a beaker and measured pH, EC using pH/ATC electrode, calibration was checked again after measuring. We had turned on the DO meter 30 min before measuring, and onsite calibrated Orion 810 with 0 and 100% stds, then measured DO in the sample and checked calibration again. We checked the mV function on the Accumet 1003 in the Zobell solution to be sure it was within 10 mV of the theorectical value, measured the sample, then calculated the Eh and rechecked the Zobell solution.

b) We collected water samples in two 2-L HDPE bottles for $\delta^{13}C$ and C/N of POC, and poisoned them with $HgCl_2$ and put them on ice. Secondly, we collected stream water in a 1 L HDPE bottle and placed it on ice immediately. Then we used $CO_2$ chamber to collect $CO_2$ efflux from the location. As soon as we put the chamber on the water surface, a syringe was used immediately to extract over 20 mL gas sample from the chamber. Then we placed a needle onto the syringe and transferred the gas to a pre-labeled (0 sec) Exetainer® vial (12 mL, vials were previously installed on a vacuum manifold and pumped until a level of 30 millitorr was reached). The vial with $CO_2$-chamber air was put on ice at once.

c) A shallow depth Backsaver® soil sampler was used to take a soil sample from 0~45 cm of the soil profile near the site. The soil sample was put into a preservation kit and labeled. Then we used chopsticks to take 2-3 submerged plant samples in the stream. They were put into another preservation kit.

We repeated steps a), b) and c) for the midstream site (about 22 m downstream) at 12:10 pm and the downstream site (about 48 m downstream) at 13:00.

After we got to the field station lab we used the hand pump to filter the two 2 L HDPE bottle for C/N of POC and $\delta^{13}C_{POC}$ through, 47 mm, Whatman glass fiber filters. Then we put the two filter papers in two boxes and labeled them at once (including my name initials, sample name, location, time, date). Then we filtered the 1 L HDPE bottle through 0.45 u filters into the following three bottles: first was a 30 mL glass vial for $\delta^{13}C_{DIC}$, poisoned it with $HgCl_2$ at once and placed on ice; second was a 250 mL LDPE/HDPE bottle for anion determination, placed it on ice; third was a 250 mL LDPE/HDPE bottle for cation determination.

Leaves from 10 terrestrial plant samples were taken along the stream bank (fig. A.4).

**Laboratory detail**

After returning to the KU Aqueous Geochemistry Lab, we transferred all the samples in the fridge at once.

On the next day, we took the filter papers out and acidified them with dilute HCl, placed them on glass plates and placed them in an oven (the glass fiber filter and glass plate had been pre-weighed), set the oven temperature to 105$^{o}$C. Then we took the terrestrial and submerged plant samples out and rinsed them with distilled-deionized (DI) water to remove dust/soil, then placed them on glass plates and put them in an oven to dry for 2-3 days at 46 $^{o}$C.

We took the terrestrial and submerged plant samples from out of the oven and transferred the water samples, plant samples, filter papers (POC), soil and gas samples to the Keck Paleoenvironmental & Environmental Stable Isotope Laboratory (KPESIL) on west campus. We ground them using a mortar and pestle with liquid nitrogen added to the sample to ensure the sample was brittle and easy to grind. Results that needed to be tested in KPESIL included C/N of

POC, $\delta^{13}C_{POC}$, $\delta^{13}C_{DIC}$, $\delta^{13}C_{CO2}$, C/N of soil samples, soil $\delta^{13}C$, C/N of terrestrial and submerged plant samples, terrestrial and submerged plant $\delta^{13}C$.

A portion of the filter paper was cut to be loaded into a 9x10mm tin capsule. Roots in the soil samples were picked out and soil samples were dried overnight and weighed. We followed the KPESIL Decarbonation Technique OM Analysis of Carbonate Bearing Samples to decarbonize soil, terrestrial and submerged plant samples. Because the samples were organic rich, we weighed 100-200 mg of samples. The decarbonation procedure is as follows: 1) We weighed the centrifuge tube without lid and recorded weights; 2) Weighed centrifuge tube without lid plus sample and recorded weights; 3) Dried samples overnight and weighed; 4) Added 30 mL of 0.5M HCl to powder in centrifuge tube slowly using the micropipette; 5) Let the centrifuge sit for 30 min to 60 min with lid on without screwing down; 6) Repeated the above steps for each sample; 7) Screwed lids tight, shook each sample for 5-15 sec vigorously; 8) Over the next 24 hours, we vented, resecured and shook each sample strongly for 5-10 sec. 9) At the end of the 24-hour period, shook all samples, put them into the "Rinse 0" tray if they don't "fizz", otherwise, put into the "Acid" tray; 10) Placed parafilm over each sample before centrifuging. 11) Centrifuged 4 samples at a time at 4000 rpm for 5-10 min starting with the "Acid" tray. 12) Poured the liquid from these samples and added 30 mL of 0.5M HCl to each tube; 13) Shook for 5-15 sec. If the sample doesn't "fizz", it goes to "Rinse 0" tray, otherwise, goes to "Acid" tray; 14) For "Rinse 0" tray, centrifuged 4 samples at a time at 4000 rpm for 5-10 min; 15) Poured liquid from sample and added 30 mLof DI water to the tube. 16) Shook robustly to make sure all sediment becomes suspended in DI solution. 17) Put these tubes in "Rinse 1" tray, repeated Steps 10-13 for "Rinse 1" samples. Then placed them in "Rinse 2" tray. 18) Centrifuged the tubes in "Rinse 2" tray. 19) Checked pH for each sample after centrifuge. Poured water if samples have pH (6-7), put them into "Oven" tray; put the acidic samples into "Rinse 1" tray. They were

rinsed again using Steps 10-13 above. 20) Threw away the lids of tubes, and put the "Oven" tray into the "Isotemp Oven" until dry. Put the entire tray in the oven at 45 $^{o}$C. 21) Weighed sample pus tube and recorded. 22) Scraped out the sample from the tube and stored the samples in small, lidded glass vials independently. We performed the KPESIL $\delta^{13}C$ and $\delta^{13}N$ measurement on a Costech ECS 4010 elemental analyzer to determine $\delta^{13}C$ of POC, $CO_2$, soil, plant and DIC; and C/N of POC, soil and plant samples.

Alkalinity was determined by titration with ~0.02 N $H_2SO_4$, with the titration end point determined as the maximum slope of the titration curve in the vicinity of pH 4.5. Other major anion concentrations (Cl, $NO_3$-N, $SO_4$) were determined by ion chromatography (KU Aqueous Geochemistry Lab, Dept. of Geology). Major cation concentrations (Ca, Mg, Na, K) were determined by ICP-OES (KU Plasma Analytical Laboratory, Dept. of Geology).

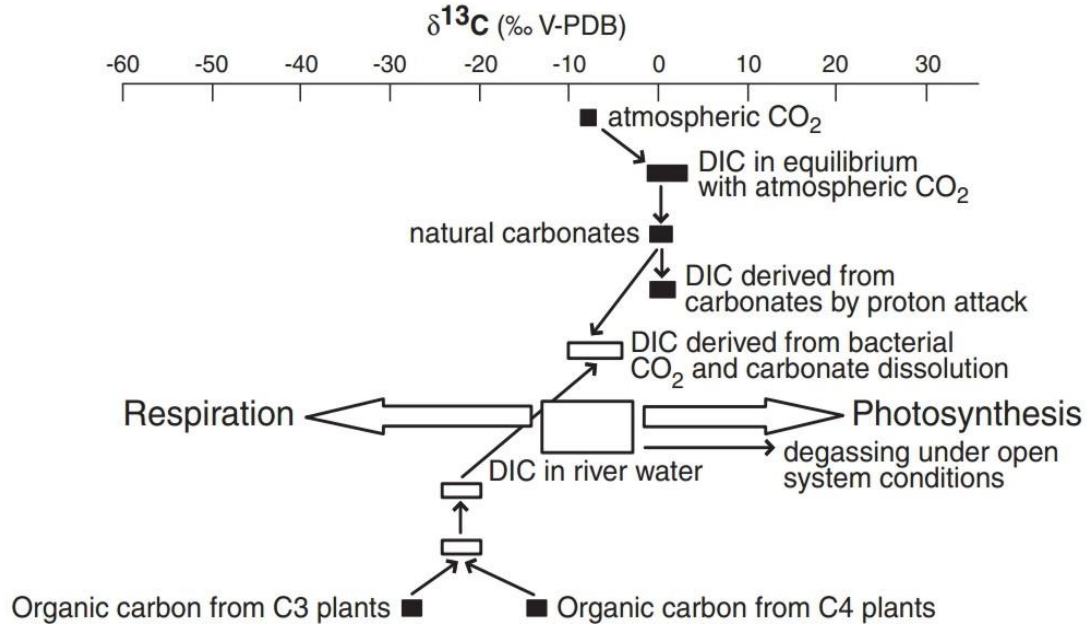


Figure A.1: Carbon isotopic signature of various components of the carbon cycle in rivers (Schulte et al., 2011).

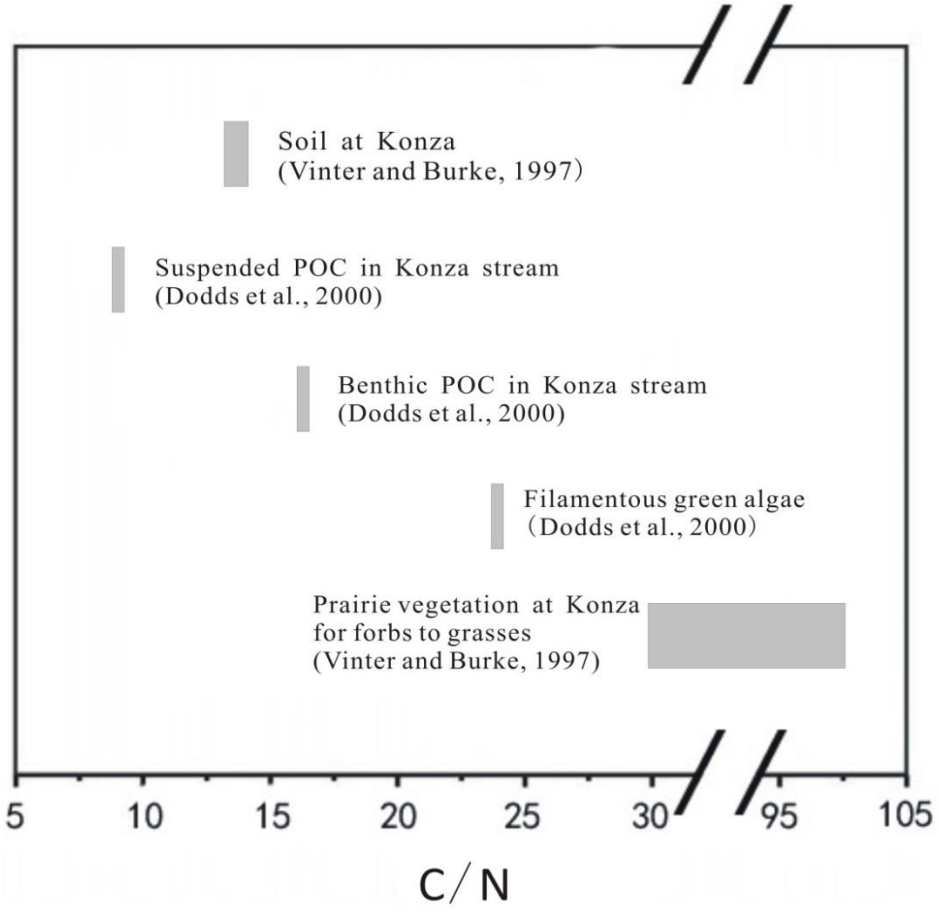


Figure A. 2: C/N values in some reservoirs at Konza Prairie.

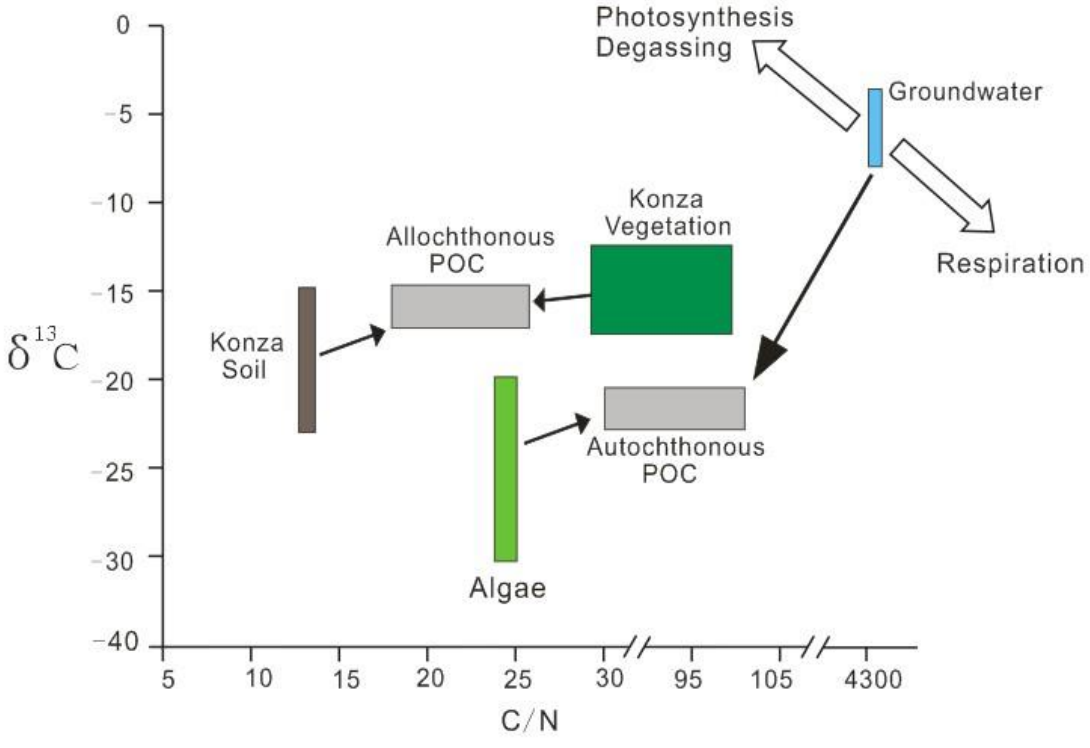


Figure A.3: Model of $^{13}C$ and C/N as co-indicator of POC sources. Black arrows represent POC forming processes. White arrows indicate the effects of processes on $^{13}C$ and C/N. Compiled from Dodds et al. (2000), Johnson et al. (2007) and Macpherson (unpublished data).


Figure A.4: 10 terrestrial samples along the stream bank.

Table A.1: Sample collection and treatment.

| **Type of sample** | **Sample container** | **Sample treatment** |
|---|---|---|
| C/N of POC | 2 L HDPE bottle | Poisoned with $HgCl_2$ immediately and filtered through pre-ashed, 47 mm, Whatman glass fiber filter |
| $\delta^{13}C_{POC}$ | 2 L HDPE bottle | Poisoned with $HgCl_2$ immediately and filtered through pre-ashed, 47 mm, Whatman glass fiber filter |
| $\delta^{13}C_{DIC}$ | 30 mL glass vial | Poisoned with $HgCl_2$ immediately and filtered through 0.45 µ disposable cartridge filter |
| Anion determination | 250 mL LDPE/HDPE bottle | Filtered through 0.45 µ disposable cartridge filter |
| Cation determination | 250 mL LDPE/HDPE bottle | Filtered through 0.45 µ disposable cartridge filter; Added with concentrated nitric acid to pH <2 |
| $CO_2$ | 12 mL exetainer vial | Stored in cold immediately |
| Plant | Preservation kit | Stored in cold immediately |
| Soil | Preservation kit | Stored in cold immediately |
| POC | HDPE box | Stored in cold immediately |

Table A.2: Methods of laboratory treatment prior to analysis.

| **Name** | **Treatment** | **Laboratory** |
|---|---|---|
| Glass-fiber filters for POC, C/N ratio and $\delta^{13}C$ | Freeze-dried; acidified with dilute HCl and oven-dried at 60 ℃ | KU AGL |
| Plant samples | Oven-dried and ground (150 mesh) | KU AGL |
| Plant C and POC | Transformed into $CO_2$ at 850 ℃ for 5 hours using the sealed-quartz tube combustion method with Cu oxide as oxidant (Buchanan and Corcoran, 1959). | K-PESIL |
| $CO_2$ | Cryogenically separated and its pressure and temperature will be measured in a sensor (Edwards Barocel 600) with a UIC CM5015 TC/TIC/TOC Coulometric Carbon Analyzer. | K-PESIL |

KU AGL: University of Kansas Aqueous Geochemistry Laboratory

K-PESIL: W. M. Keck Paleoenvironmental and Environmental Stable Isotope Laboratory

Table A.3: Methods of laboratory analyses.

| **Analysis** | **Method** | **Laboratory** |
|---|---|---|
| C/N ratio | Elemental analyzer | KPESIL |
| $\delta^{13}C$ of $CO_2$ (DIC, POC) | Isotope ratio mass spectrometer | KPESIL |
| $CO_2$ | Gas chromatography | KPESIL |
| Alkalinity | Titration | KU AGL |
| Anions | Ion chromatography | KU AGL |
| Cations | Optical emission spectroscopy | KU PAL |
| pH, temp., DO, SC, Eh | Individual meter and probe | On site |
| DIC, $pCO_2$, SIc | PHREEQC Interactive | |

KPESIL: Keck Paleoenvironmental and Environmental Stable Isotope Laboratory

KU AGL: University of Kansas Aqueous Geochemistry Laboratory

KU PAL: University of Kansas Plasma Analytical Laboratory

## Appendix B. Floating $CO_2$ chamber

The chamber for Konza sampling was made from a ~5L plastic bucket and a ~1L polyethylene container. The chamber has an inner diameter of 21 cm at the end sitting in the water. The chamber wall extended approximately 3 cm into the water to keep the gas from leaking from the side. Gas samples of the air enclosed by the chamber were withdrawn by a syringe through a butyl rubber stopper on the top of the chambers immediately after placing them on the water surface, and again at a 1-min interval for another four times to the end of the measurement period.

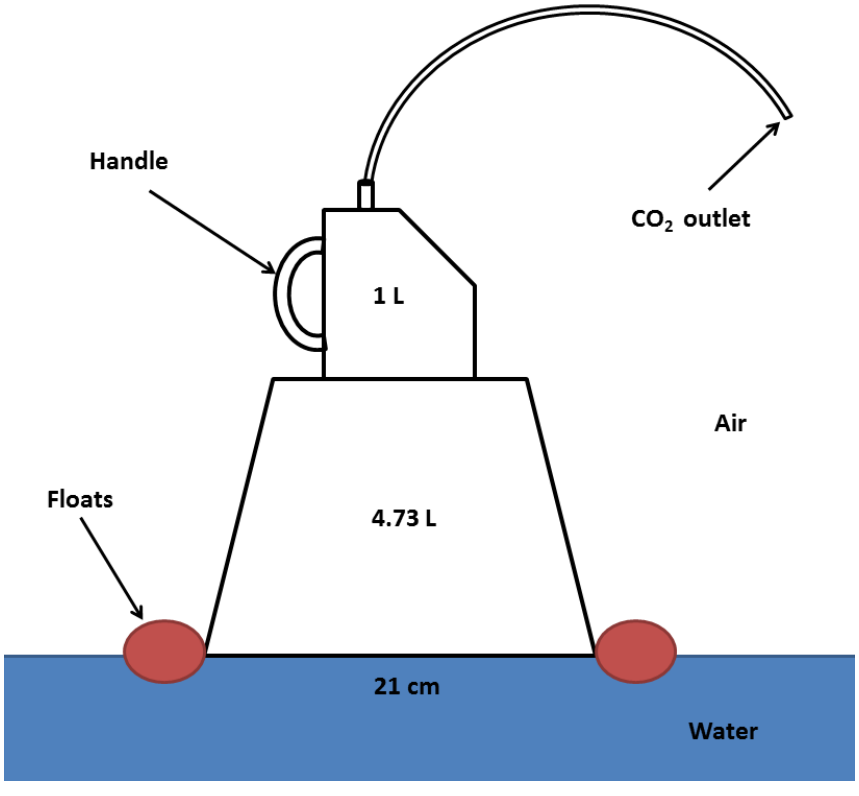


Figure B.1: Floating chamber used in Konza.

The chamber for Maolan sampling was made from a 14 L plastic bucket. The chamber has an inner diameter of 40 cm. The chamber wall extended ~3 cm into the water to keep the gas from leaking from the side. Gas samples of the air enclosed by the chamber were withdrawn by a syringe through a butyl rubber stopper on the top of the chambers immediately after placing them on the water surface, and again at a 2-min interval for another four times to the end of the measurement period.

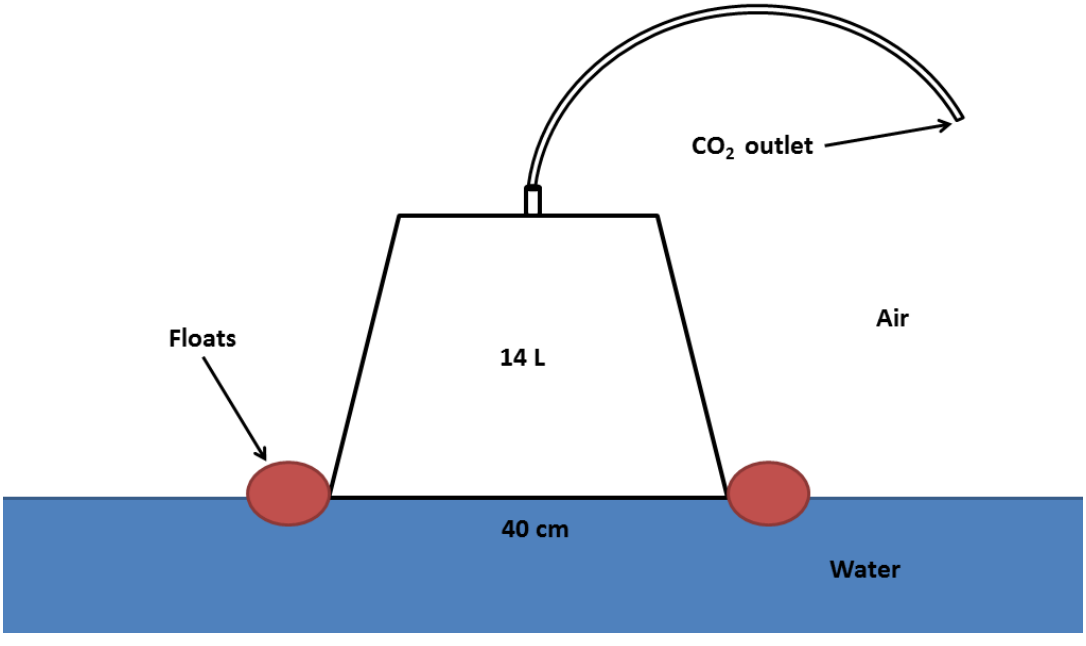


Figure B. 2: Floating chamber used in Maolan.

$Flux(mg/s/m^2) = 0.001963*(dc/dt)*(V/A)*(273.15/T_m)*(P_m/101.325)$

$Flux(mg/h/m^2) = 7.069*(dc/dt)*(V/A)*(273.15/T_m)*(P_m/101.325)$

$Flux(mg/d/m^2) = 169.6*(dc/dt)*(V/A)*(273.15/T_m)*(P_m/101.325)$

where dc/dt: increase rate in $CO_2$ partial pressure in the floating chamber; V: chamber volume; A: chamber bottom area; 273.15: standard temperature in K; $T_m$: the measured temperature of the sampling day in K; $P_m$: the measured pressure on the sampling day in kPa; 101.325: standard pressure in kPa.

## Appendix C. Long-term data analysis of Konza Prairie

### Summary

This study continues and expands the work of Macpherson et al., (2008), who proposed several hypotheses clarifying the increasing trend of shallow groundwater $pCO_2$ at the Konza Prairie LTER Site. Approximately monthly data over 20 years at the Konza Prairie in northeastern Kansas shows strong connection between the annual cycles of air temperature, precipitation, atmosphere $pCO_2$, and groundwater $pCO_2$ trends.

The seasonal trend of groundwater $pCO_2$ mimics the temperature annual cycle because temperature governs soil $CO_2$ (the main source of groundwater $CO_2$) by controlling the terrestrial vegetation photosynthesis and root respiration. Kings Creek discharge shows abrupt variation with precipitation, while there is three months of lag-time between groundwater $CO_2$ maximum and precipitation. The delay may be the delivering time of soil $CO_2$ to the groundwater initiated by storm events. Analysis from SPSS shows that atmospheric temperature is the greatest factor regulating groundwater $CO_2$. NPP shows some fluctuation with precipitation and air temperature. But it seems to be non-responsive to other parameters and shows no significant pattern over the study period at the Konza Prairie. Results show that groundwater $CO_2$ has increased about 29% from 1990 to 2009 at Konza Prairie, which is greater than the 9% increase in atmospheric $CO_2$ over the same time period, indicating that shallow groundwater is performing as a $CO_2$ sink.

### C.1. Introduction

The Konza Prairie Long-Term Ecological Research (LTER) Site and Biological Station (Konza), located in the northeastern Kansas, is isolated from cities and agriculture croplands. Thus, Konza is an ideal place to study natural grassland communities and ecosystems. Long-term studies would serve to understand how the global change phenomena including land-use and

land cover, climate and hydrologic change, nutrient enrichmenton influence the sustainability and dynamics of grassland ecosystems.

Konza is categorized by shallow groundwater depth and comparatively thick soil depth (Tsypin and Macpherson, 2012). For shallow groundwater, soil is the principal source of $CO_2$ and soil $CO_2$ dynamics are the result of photosynthesis and root respiration, moisture, and matrix. It has been shown that downward transport of $CO_2$ at the Konza is favored in mid-summer, so long as moisture is present, in the form of diffuse flow, and storm events dilute groundwater rather than cause entrapment of soil gas with downward piston-flow downward (Tsypin and Macpherson, 2012). Processes in the soil affecting $CO_2$ production, then, also affect groundwater chemistry. In general, short-term events like storm or drought and long-term events such as karst processes, global warming and expansion of woody vegetation are important factors influencing the belowground carbon cycle. For this study, we consider some of these factors over the relatively short period of 19 years, for which we have groundwater chemistry. We use the water chemistry of the same two wells, 6.3 m and 12.6 m deep, producing from a shallow limestone aquifer, used by Macpherson et al. (2008). That study presented the results of a 15-year study period (1991-2005), concluding that groundwater $pCO_2$ increases were higher (18-36%) than the atmospheric $pCO_2$ increase (around 7%) over that time period. That study also showed the similarity of the periodicity of atmospheric $CO_2$ with groundwater $CO_2$, and presented statistical evidence for the significance of the groundwater $CO_2$ increase. In this study, we include that data set and extend it to 2009, and investigate statistical correlations among the groundwater $CO_2$ trends, air temperature, meteoric precipitation, and stream discharge, in an effort to discover the major driving factors for the periodicity and long-term increase in groundwater $CO_2$.

Several explanations for the increased belowground $CO_2$, such as longer groundwater residence time, increased atmospheric nitrogen loading, and increased soil $CO_2$ due to higher

rates of organic matter decomposition have been considered (Macpherson et al., 2008). The driving mechanism for rising belowground $CO_2$ is still not clear, but it is not linked to groundwater residence time caused by drought, or increased nitrogen in precipitation accelerating the vegetation-controlled carbon cycle (Macpherson et al., 2008). In another study, a two-year experiment on a temperate heathland suggested that belowground processes responded significantly to manipulation of rainfall, temperature and atmospheric $CO_2$ concentration, but the response to the combined factors manipulation was not well predicted by the responses to the individual factor manipulation (Andresen et al., 2010). This suggests that a single factor does not unambiguously express the ecosystem responses to complicated forcings (Andresen et al., 2010). Still, because soil must be the single largest source of $CO_2$ in shallow groundwater, processes affecting soil $CO_2$, such as degradation of organic matter and soil respiration, require further investigation of linkages to groundwater $CO_2$, especially since global soil respiration rates may be increasing along with global atmospheric temperature (Bond-Lamberty and Thomson, 2010).

This study considers variations in approximately monthly data (water chemistry, precipitation, atmospheric $pCO_2$, temperature, groundwater $pCO_2$, discharge and net primary production) over 19 years at the Konza Prairie in northeastern Kansas. The aim of the research is to understand if there is a dominant factor linked to the groundwater $pCO_2$ annual cycle. Although causation cannot be proved with this method, coincidence of trends may be helpful in predicting the groundwater $CO_2$ trend under current warming conditions.

## C.2. Study area

### C.2.1. Location

The Konza is located in the Flint Hills region of northeastern Kansas ($39^{o}05$N, $96^{o}35$W), approximately 13 km south the city of Manhattan (fig. C.1). The site occupies 34 $km^2$ of the

northern part of the Flint Hills physiographic province and includes 60 3$^{rd}$ to 4$^{th}$-order watersheds. Since 1991, the lower one-third of an upland watershed (N04d), about 1.2 km$^2$ in area, has been used for approximately monthly monitoring of groundwater chemistry and water table elevation. N04d is located on the watershed divide between Kings Creek and Deep Creek to the east and the southern part of McDowell Creek to the south. Kings Creek, the main stream draining the Konza Prairie LTER Site, is a tributary to the Kansas River. It empties into McDowell Creek north of the Konza Prairie LTER Site.

The Kings Creek Basin lies within Riley County. All but the lowest part of Kings Creek is entirely within the Konza LTER Site, so the basin is marginally affected by human activity. Contamination of groundwater at N04d by agricultural chemicals is not likely, because the closest agriculture region, about 5 km away, is separated by a local watershed divide (Tsypin and Macpherson, 2012). Topographic relief in the N04d watershed is about 60 m and the elevation at the weir monitoring stream from the watershed is 364 m. The topography is gently rolling and the type and depth of soil varies with topographic position. Hilltops are flat and gradients on the hill slopes are 10-25%.

### C.2.2. Climate and vegetation

The climate at Konza is typical, temperate mid-continental. In this region the variability in precipitation and temperature is high within and between years (Hayden, 1998). Yearly mean air temperature is 13 ℃. Summer is usually warm and wet, while winter is cold and dry. Average monthly temperature ranges from 2.7 ℃ in January to 26.6 ℃ in July. Average total annual precipitation is 835 mm, based on a 30-year record from 1950-1980 at nearby Manhattan, KS, with 75% falling during the growing season, April through October. May and June are months with the highest average precipitation, accounting for 30% of the annual amount, although

storms can occur during any time. Konza Prairie typically has 200 to 300 hours of intense thunderstorms in a year (>56mm/hr) (Hayden, 1998). The dominant source of the precipitation during the growing season is Gulf-of-Mexico-derived moist maritime tropical air from the south and southeast. Summer rainfall characteristically arises from thunderstorms associated with fronts and squall lines in the region (Hayden, 1998). In the non-growing season, the precipitation source is Arctic and continental polar air masses from the north and west. Mean annual total snowfall is 521 mm with January typically receiving the highest snowfall, averaging 150 mm.

Konza is an unplowed native tallgrass prairie. The tallgrass canopy reaches over 2.5 m in height in the most productive years. The vegetation at the site is mostly perennial, warm-season C4 grasses, predominately big bluestem, little bluestem, Indiangrass and switchgrass. Less abundant species include warm-season and cool-season grasses, composites, legumes, and other forbs. Buchbrush and smooth sumac are examples of common woody species (Freeman, 1998; Towne, 2002).

**C.2.3. Geology**

The bedrock underlying Konza Prairie is composed of Early Permian couplets of limestone and shale (fig. C.2). Limestones form flat uplands and hillside benches, while shales form slopes with 10-25% gradients. At the N04d watershed, bedrock is exposed at the surface on parts of the uplands and hillside benches, but otherwise covered by thin Quaternary deposits. The focus of this study is the Morrill Limestone Member (Morrill) of the Beattie Limestone (Oviatt, 1998). The Morrill is a shallow marine limestone with a sharp base and transitional top (Twiss, 1988). Solution enlargement of joints in the Morrill has created an aquifer that yields small to moderate amounts of water to wells. The Morrill is underlain by the ~3 m thick Florena Shale, the, middle member of the Beattie Formation, a calcareous, gray deep-water shale. The Morrill is

overlain by the ~4.5 m thick Stearns Shale, a calcareous, terrigenous to marine shale (Zeller, 1968).

### C.2.4. Soils

Soils of Konza are generally poor with carbonate and has low to moderate cation exchange capacities (typically less than 40 meq/100g) (Ransom et al., 1998). The soils are less than 1 m thick, evolving on loess, limestone and shale (Macpherson et al., 2008). Soils at N04d watershed are relatively deep and temperately well-drained. The moderately permeable soils are located on foot slopes and valley bottoms. The organic content declined with depth from 6% to lower than 1%. The clay content ranges from 26 to 39%, silt from 37 to 57%, and sand from 7 to 40%. Soils commonly contain low amount of nutrients (3.5-6.0 ug/g available P, 265-285 ug/g K, and 2.0-6.0 ug/g $NO_3$-N) (Wehmueller et al., 2005).

### C.2.5. Hydrogeology

The neo-karst aquifers include the Morrill Limestone Member of the Beattie Limstone and the upper and lower portions of the Eiss Limestone Member of the Bader Limestone (Macpherson, 1996). Thus, the aquifers are like sandwich (White, 1969). The aquifers in this region are the 1-2 m thick limestone layers and the alluvial deposits, displaying secondary porosity (Macpherson et al., 2008). The conductivities of the aquifers range from $10^{-8}$ to $10^{-3}$ m/s (Pomes, 1995). The aquitards are the thicker shale layers.

The connection between surface water and groundwater is fairly rapid. Water level and temperature change within a few hours after precipitation (Macpherson, 1996). During a single sampling even in 1991, the tritium levels of groundwater are similar to meteoric precipitation (Macpherson, 1992). Water level oscillates on a diel cycle with ~1 cm during prolonged dry

times in the growing season. Water level starts to decrease soon after sunrise, and rises again within a few hours after sunset (Kissing and Macpherson, 2006).

The water chemistry of shallow groundwater ($Ca^{2+}$ and $HCO_3^-$ type) in the N04d watershed is similar. $Mg^{2+}$ is higher than in others in some units, with infrequent peaks of $SO_4^{2-}$. The major control on groundwater pH and alkalinity is soil and bedrock carbonate weathering (Macpherson, 1996).

## C.3. Methods

The sampling took place in the northern part of the N04d watershed at Konza. Observation wells are made of 5-cm diameter PVC casing with a 61-cm PVC slotted well screen at the bottom. Steel well protectors protect the wells from controlled burning of the grassland every four years and damage from bison. Two wells of the total of 35 wells in the watershed are presented in this study. Well 4-6 Mor is 12.6 m deep, while well 3-5 is 6.3 m deep. Both wells have been sampled continuously over the study period. We also present the relation between stream samples collected at two locations nearest to the two wells. Sampling and chemical analysis of groundwater and stream water occurred every four to six weeks. Details of sampling and analysis methods are given in Macpherson et al. (2008).

### C.3.1. Geochemical speciation modeling

Saturation index of carbonate minerals and dissolved inorganic carbon (DIC) species are controlled by measured pH, alkalinity, and other dissolved species. Accurate pH measurements are difficult at the study site because the limestones are low-yield aquifers and there is no power available to run a pump. In this study, we follow the method in Macpherson et al. (2008). In brief, pH was determined using the deliberate-degassing bottle technique (DDB pH; described in detail

in Macpherson, 2004) over a 1.67-year period to establish the annual cycle of calcite saturation. This annual cycle was used, in all other years, to predict pH, $pCO_2$ and other speciation with PHREEQC Interactive 2.18.5570, applying the PHREEQC database (Parkhurst and Appelo, 1999). Headspace $CO_2$ samples and field pH were determined in 2005 to investigate the validity of using a repetitive SIc annual cycle. The measured results correspond well with predicted $pCO_2$ and pH (Macpherson et al., 2008). The full chemical analysis and SIc are input in PHREEQC to calculate the pH and the partial pressure of $CO_2$.

### C.3.2. Other data

Net primary production (NPP) data was acquired from the Konza LTER website (www.konza.ksu.edu). At Konza, since 1989 aboveground NPP of Tallgrass Prairie has been evaluated at maximum standing crop biomass on three watersheds (001d, 004b, 020b). Because soils of N04d watershed are mostly Tully type, Tully soil was chosen as representative of the N04d watershed. The NPP of live grass and forbs were combined for this study. Because the NPP data of some of the months are missing and September is the only month for which NPP data is available for all the years, only the NPP data for September is used here to represent the value for each year.

### C.3.3. Data analysis

In order to investigate the relationship between the parameters, it is necessary to examine the lag time between two parameters (atmospheric $CO_2$ and temperature; groundwater $CO_2$ and temperature; groundwater $CO_2$ and atmospheric $CO_2$, groundwater and meteoric precipitation). We plot the data and correlate the peak values for each pair of parameters every year, and estimate the lag time between the two peaks for each year. The average lag time each year for all

of the years is used as a lag time for those two parameters. Linear regression analysis in IBM SPSS Statistics version 21 was used to evaluate the most significant parameters affecting groundwater $CO_2$. Groundwater $CO_2$ was input as a dependent factor; air temperature, atmospheric $CO_2$ and meteoric precipitation were independent factors.

## C.4. Results

### C.4.1. Water chemistry

The study period for well 3-5 and well 4-6 is from 22 May 1990 to 7 July 2009. The chemistry of water in the two wells is very similar. Total dissolved solids is composed primarily of titration alkalinity, calcium and magnesium 82-94% (by weight). In well 3-5, alkalinity occupies 87-99% of the total carbon. The pH ranges from 7.18 to 8.06 and TDS varies from 204 ppm to 388 ppm. For well 4-6, alkalinity makes up 84-99% of the total carbon, and pH fluctuates between 7.03 and 8.01. TDS oscillates between 113 ppm to 375 ppm.

### C.4.2. Atmospheric $CO_2$

We use the time series of atmospheric $CO_2$ recorded at the Mauna Loa Observatory (MLO) situated on the island of Hawaii, because it was designed and has been continually verified to capture the global average atmospheric $CO_2$ trend. The atmospheric $CO_2$ at MLO is similar to that measured at Niwot Ridge, which is the nearest station to the Konza, but which has a shorter record. The annual cycle of air $CO_2$ at the MLO records the effects of photosynthesis and respiration (Buermann et al., 2007) of the northern hemisphere biosphere, with a maximum at the start of the growing season (April/May) and a minimum at the end of the growing season (September/October) (fig. C.3).

### C.4.3. Long-term trends

Fig. C.4 displays the long-term trends (year 1991 to 2009) of atmospheric $pCO_2$, groundwater $pCO_2$ and alkalinity as $HCO_3^-$ concentration for well 3-5. All of the parameters increase at least 0.5% annually. Among them, groundwater $pCO_2$ increases at the highest rate of 184 ppmv yearly, about 1.6%, while the atmospheric $pCO_2$ increases at 1.84 ppmv annually (0.5%). Alkalinity rises at a rate of 2.5 ppm/a. Atmospheric $pCO_2$ increased by 9% from 1991 to 2009. Over the same time period, groundwater $pCO_2$ increased by about 29%.

### C.4.4. Groundwater $pCO_2$ in relation to other physical parameters

Fig. C.3c shows that groundwater $pCO_2$ fluctuates on an annual cycle, similar to the atmospheric $pCO_2$ cycle from year 1991 to 2009. However, there is about a 5 to 7-month lag time between both their maxima and minima. The atmospheric $pCO_2$ is normally the highest in May, while the groundwater $pCO_2$ usually reaches its maximum in September to October. The atmospheric $pCO_2$ decreases to its annual minimum in August to September, and groundwater $pCO_2$ decreases to its annual minimum in February to April.

Fig. C.3b displays that groundwater $pCO_2$ corresponds very well with air temperature. There is about two months lag time between the two parameters. Temperature increases to its maximum value in July or August, and decreases to its lowest value in January.

Fig. C.5b shows that groundwater $pCO_2$ and prairie precipitation follow similar annual trends, with a time lag between them. The greatest amount of precipitation and discharge usually occur in May to July. Generally, groundwater $pCO_2$ increases with rising precipitation after around three month.

### C.4.5. Net primary production

Sala et al. (1988) estimated that annual aboveground NPP should average 510 g/m$^2$ at Konza. September is the month which NPP data are available in every year. The average NPP for September is 420 g/m$^2$, suggesting that NPP is normally the highest in early fall. NPP data for September is used to represent the value for the year (fig. C.6). The NPP values range from 310 g/m$^2$ to 538 g/m$^2$. There is no clear pattern of the NPP variation in relation to most of the parameters, but the NPP commonly reaches its annual maximum after precipitation peaks (fig. C.6b), and right after the air temperature peak (fig. C.6a). Aboveground NPP from 1991 to 2005 shows high variability and no statistically defensible trend.

## C.5. Discussions

### C.5.1. Implication from SPSS

Data of the three important factors (temperature, atmospheric $CO_2$ and rainfall) that could potentially influence the groundwater $CO_2$ were input in SPSS to evaluate their significance. GW $CO_2$ is used as a dependent factor and the three parameters are as independent factors. “Enter Method” in the Linear regression was chosen as the analytical method. After adjustment for the lag time, we could generally correlate the data of each parameter to groundwater $CO_2$. Results show that rainfall has the highest sig. of 0.244, meaning it is the least influential factor, and therefore should be excluded (normally if the sig. is less than 0.05 the effect is significant). Temperature is the most dominant factor on groundwater $CO_2$ with the lowest sig. (0.000), followed by atmospheric $CO_2$ (sig. 0.003)

### C.5.2. Controlling factors on groundwater $pCO_2$

#### C.5.2.1. Temperature and atmospheric $pCO_2$

The oscillation of $CO_2$ in the northern hemisphere reflects that photosynthesis uptaking $CO_2$ and respiration releasing $CO_2$ are not simultaneous (Buermann et al., 2007). During the summer, photosynthesis dominates over respiration in the northern hemisphere, resulting in temporary storage of carbon in plant tissues along with a seasonal decline in atmospheric $pCO_2$ levels. Therefore, the minimum atmospheric $CO_2$ usually occurs in the early fall each year. On the other hand, in winter, respiration by decomposers exceeds photosynthesis, because many plants are dormant or leafless. Thus, atmospheric $pCO_2$ returns to the highest levels. The continuous $CO_2$ increase in the atmosphere from 1991 to 2009 is mostly due to the burning of fossil fuels, but a substantial portion has also resulted from the destruction of plant biomass. A study points out that although fast-growing vegetation is found on most areas that are harvested, the degree of carbon buildup does not match the rate of carbon loss during harvest, indicating a net carbon transfer from biomass to atmosphere (Harmon et al., 1990). The increased atmospheric $pCO_2$ levels should not directly influence the groundwater $pCO_2$, because belowground $pCO_2$ levels are normally one to two orders of magnitude higher than atmospheric $pCO_2$ (Macpherson et al., 2008). However, the groundwater $pCO_2$ wave mimics the atmospheric $pCO_2$ and temperature cycles, and $pCO_2$ build-up in the shallow aquifer is much faster than the atmospheric $pCO_2$ growth. Temperature and soil moisture are the main controls on terrestrial vegetation photosynthesis (where light is not limiting) and root respiration. Therefore the atmospheric $pCO_2$ is related to air temperature, but only coincidentally related to groundwater $CO_2$ variation.

Belowground $CO_2$ mostly derived from soil. $PCO_2$ in the groundwater peaks during the late fall, which is typical timing for shallow aquifers (Macpherson et al., 2008). Shallow soil

$pCO_2$ peaks in the summer and there is a greater lag time to maximize $CO_2$ with increasing soil depth (Hendry et al., 1999; Tsypin and Macpherson, 2012). After the maximum, the soil $CO_2$ declines due to moisture deficiency in the late summer and temperature drop beginning in the fall. The $CO_2$ begins decreasing earliest in the shallowest part of the soil and latest in the deepest part (Tsypin and Macpherson, 2012). Groundwater $pCO_2$ peaks in October, thus, the 2-3 months of lag-time between the soil and groundwater $CO_2$ may be the delivering time of soil $CO_2$ to the groundwater. This explains the out of phase between $pCO_2$ in groundwater and temperature.

Temperature and soil moisture determine soil $CO_2$ (the main source of groundwater $CO_2$), thus, the seasonal trend of temperature and groundwater $pCO_2$ are similar (fig. C.3).

### C.5.2.2. Prairie precipitation and Kings Creek discharge

The aqueous geochemistry in the aquifers is related to the history of precipitation events (including magnitude) and temporal relation to earlier events (thus controlling groundwater residence time). The connections between stream and groundwater at Konza Prairie are complicated by sporadic and unevenly sized precipitation events (Gray et al., 1998).

At the Konza Prairie, Kings Creek discharge rate shows immediate variation, usually less than a month, with precipitation (fig. C.5a). This rapid response has two implications. Firstly, it suggests that the rain water travels quickly to the groundwater and discharges the stream as base flow, which is a characteristic of karst systems. Secondly, intense precipitation events dominate river and stream discharge when runoff is rapid (Milly et al., 2002). Therefore, groundwater might be bypassed if intense precipitation events dominate stream discharge by rapid runoff.

Because rain water moves down from the large porous media, but most of the $CO_2$ in the soil is trapped in the small pores, thus, the $CO_2$ downward movement is a lot slower than rain water. Tsypin and Macpherson (2012) studied the extreme precipitation events at Konza Prairie

and showed that large rainfall dilutes groundwater instead of initiating entrapped $CO_2$ downward movement. This might be the reason for the delayed response of $pCO_2$ to recharge and the most intense precipitation does not necessarily result in the greatest $pCO_2$. Liu et al. (2007) discovered that during storm events, the dilution effect controls the variations by decreasing both conductivity and calcite/dolomite saturation of the springs in southwest China.

**C.5.3. Net primary production**

The annual accumulation of organic matter per unit of land is a measure of NPP, however, it is not directly equivalent to plant growth as measured by ecologists. Some part of the NPP is lost to herbivores and litterfall. NPP usually increases as a function of intercepted radiation (Runyon et al., 1994), but photosynthesis normally captures only 1% of the total energy from sunlight (Reiners, 1972).

The methods for estimating aboveground NPP are well established for grasslands (Singh et al., 1975). Belowground biomass is higher than aboveground biomass, and grasslands distribute more production below ground than above ground when compared with forests, but belowground NPP is hard to estimate and is usually considered as proportional to aboveground NPP (Macpherson et al., 2008). At Konza Prairie, NPP estimation has been made since 1989 only at maximum standing crop biomass.

Researchers have noted that photosynthesis will be stimulated by greater $CO_2$ delivered to the enzyme ribulose bisphosphate carboxylase as the $CO_2$ levels in atmosphere rise, causing the NPP of land vegetation to increase (Amthor, 1995). This corresponds to Konza NPP data that the peak of standing crop biomass normally occurs in September, soon after the air temperature peak (fig. C.6a). The growth of vegetation is limited by many other factors, and $CO_2$ may have little long-term direct influence (Thomas et al., 1994). The controlling parameters are location specific

and not common across soil types and vegetation types, but may be linked to the dynamics and limiting factors of the organisms (Briones et al., 2009). Sala et al. (1988) also noted that precipitation was related strongly to aboveground NPP ($r^2$=0.90) across grassland sites. At Konza, NPP does show some fluctuation with precipitation but it has shown no statistically significant change (fig. C.6b) under ambient conditions, although NPP trends are difficult to recognize (Tate and Ross, 1997).

**C.6. Conclusions**

The connections between annual cycles of groundwater $CO_2$, atmospheric $CO_2$, air temperature, precipitation, and net primary production are examined at the N04d watershed at the Konza Prairie LTER Site from 1990 to 2009.

SPSS results show that air temperature is the main control of groundwater $CO_2$ seasonal cycle, while rainfall is the least influential factor on groundwater $CO_2$. The seasonal trend of air temperature, atmospheric $CO_2$ and groundwater $CO_2$ are alike. Air temperature controls the terrestrial photosynthesis and respiration, therefore, it determines both atmospheric $CO_2$ and soil $CO_2$ (main source of groundwater $CO_2$). Kings Creek discharge shows instant change with precipitation. The 2-3 months delay time between precipitation and groundwater $CO_2$ maximum might be the travel time of soil $CO_2$ to the groundwater initiated by large precipitation events. The most intense precipitation does not necessarily result in the greatest $pCO_2$. NPP shows some fluctuation with precipitation and air temperature. But it has shown no statistically significant change under ambient conditions from 1991 to 2005, although NPP trends are difficult to identify.

The magnitude of groundwater $CO_2$ increase (about 29%) is much higher than that of the atmospheric $CO_2$ (about 9%) during the same time period. We conclude that shallow

groundwater is acting as a $CO_2$ sink because $CO_2$ build-up in the shallow aquifer is much faster than the atmospheric $CO_2$ growth.

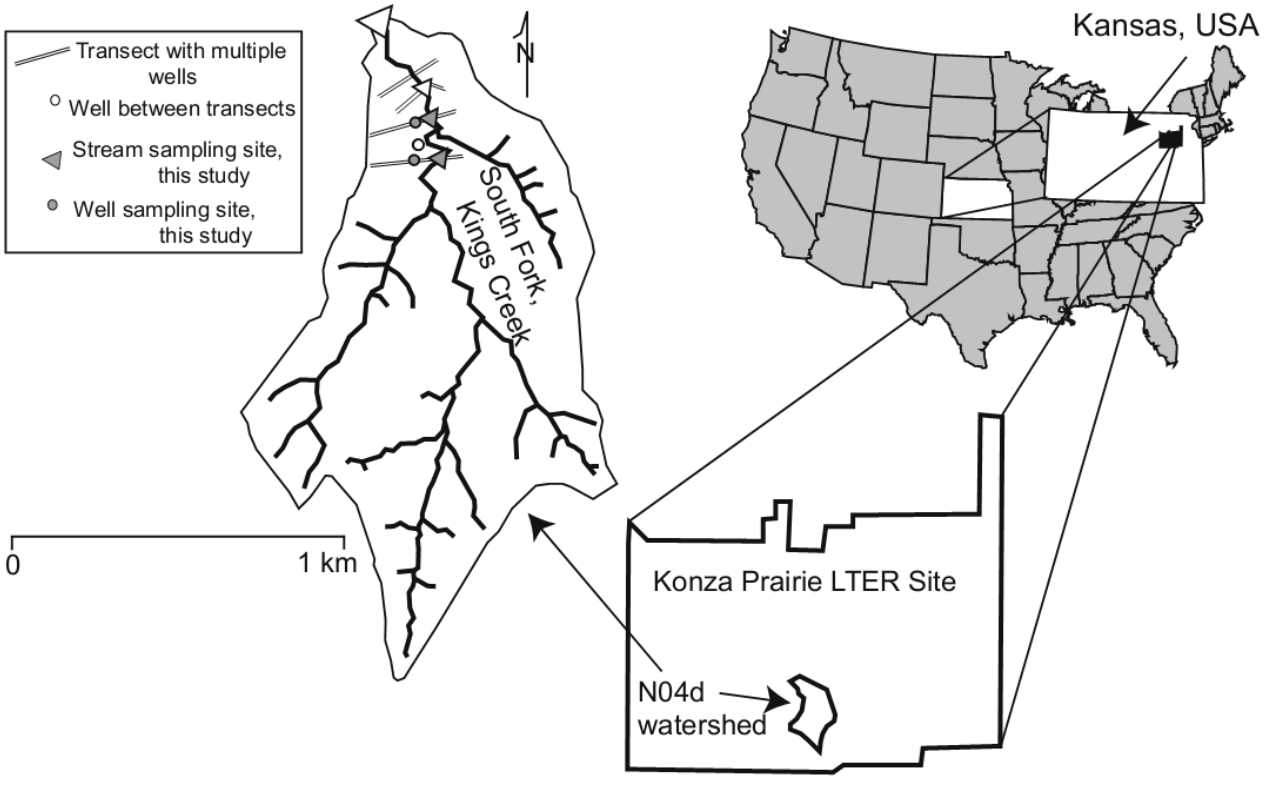


Figure C.1: Geographic location of the Konza Prairie LTER Site (Macpherson et al., 2008).

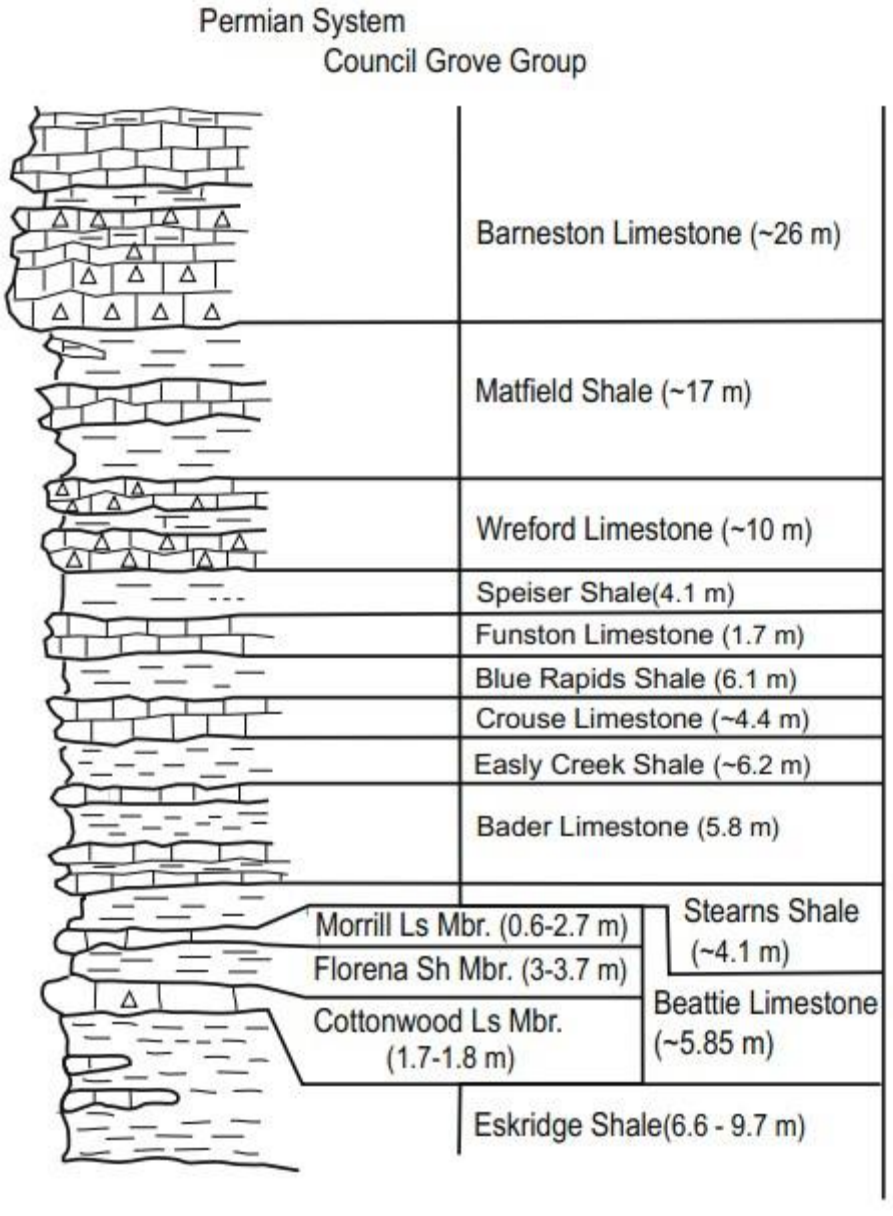


Figure C.2: Stratigraphic column of the study area; the Morrill Limestone Member is the aquifer investigated in the study. (Macpherson et al., 2008).

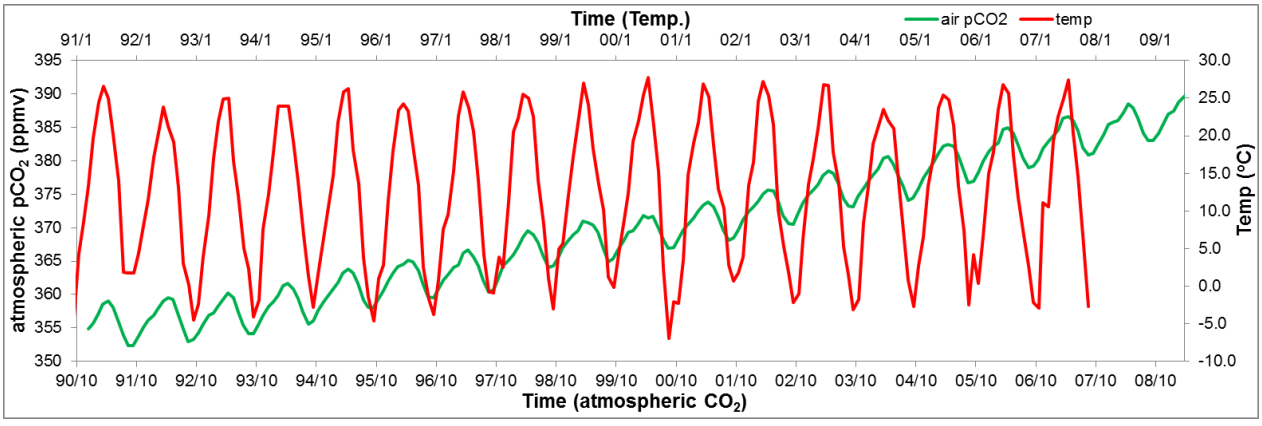


**(a)**

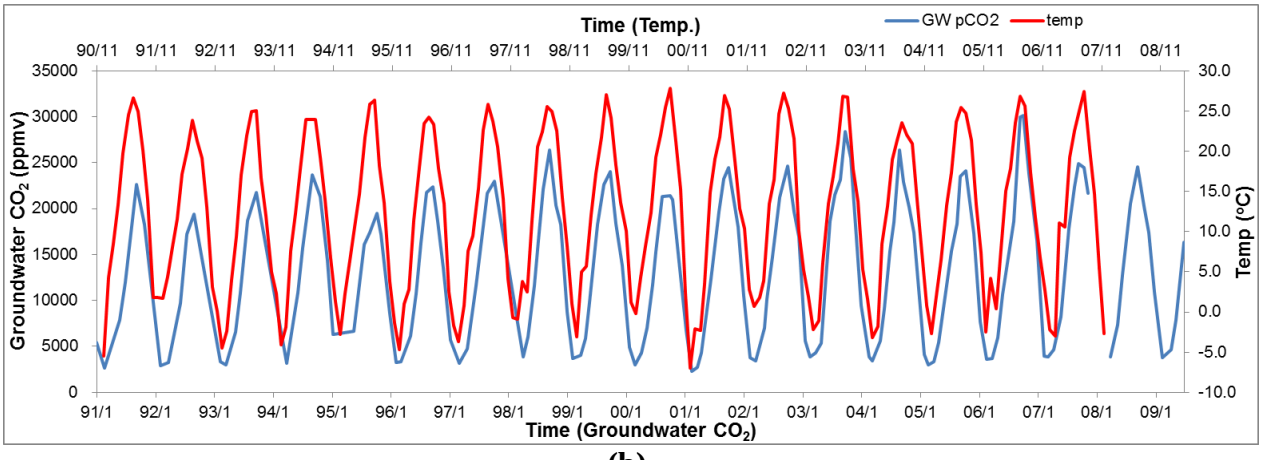


**(b)**

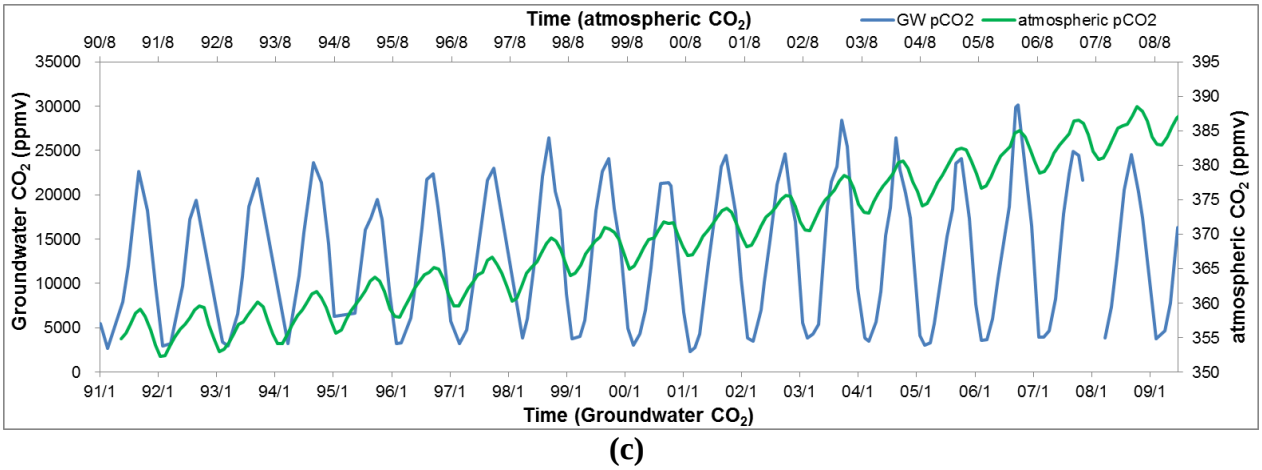


**(c)**

Figure C.3: Relation between atmospheric $CO_2$ and temperature (a), time-lagged groundwater $CO_2$ and temperature (b), groundwater $CO_2$ and atmospheric $CO_2$ (c) for well 3-5.

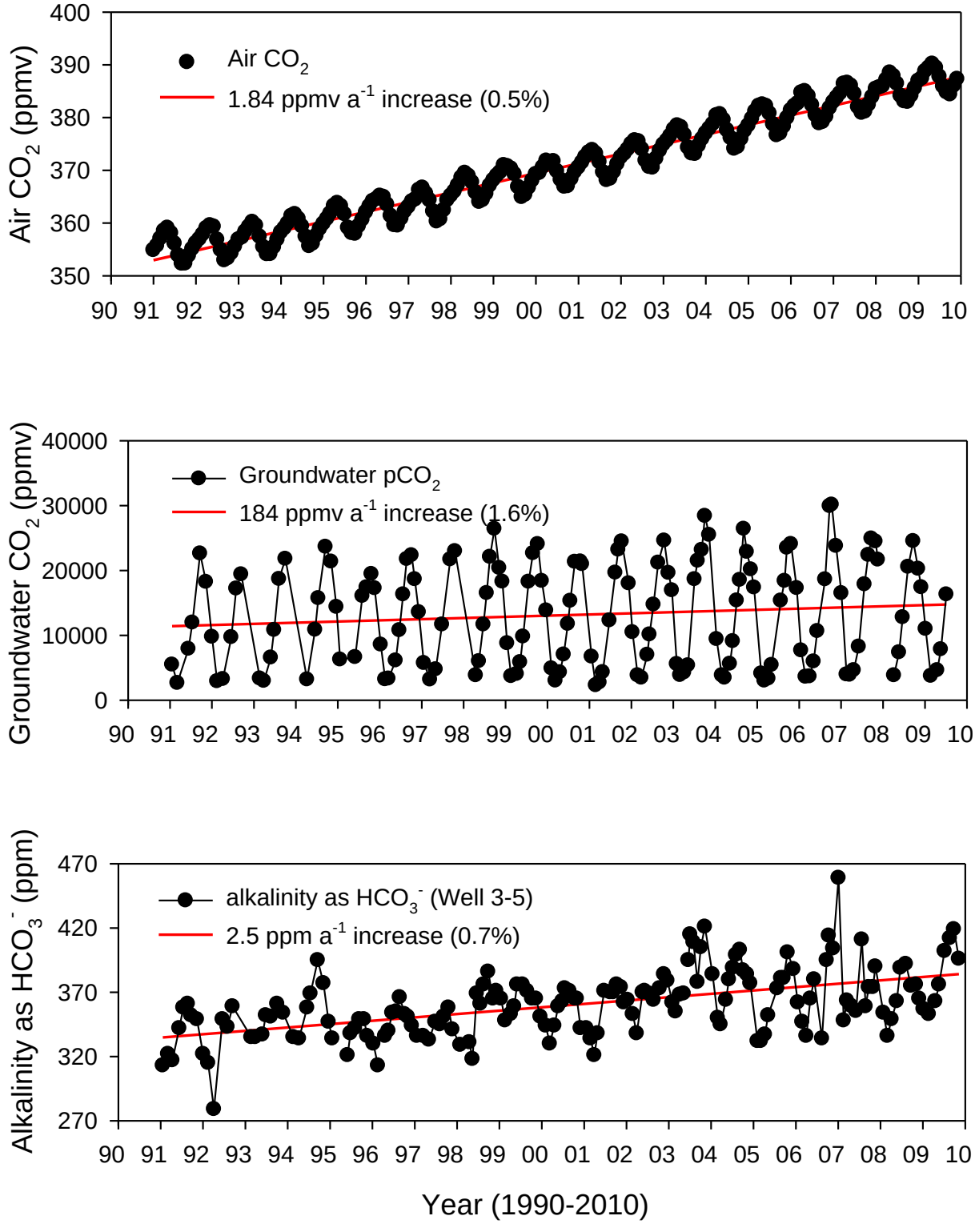


Figure C.4: Long-term trends of atmospheric $pCO_2$groundwater $pCO_2$ and alkalinity as $HCO_3^-$ concentration of well 3-5.

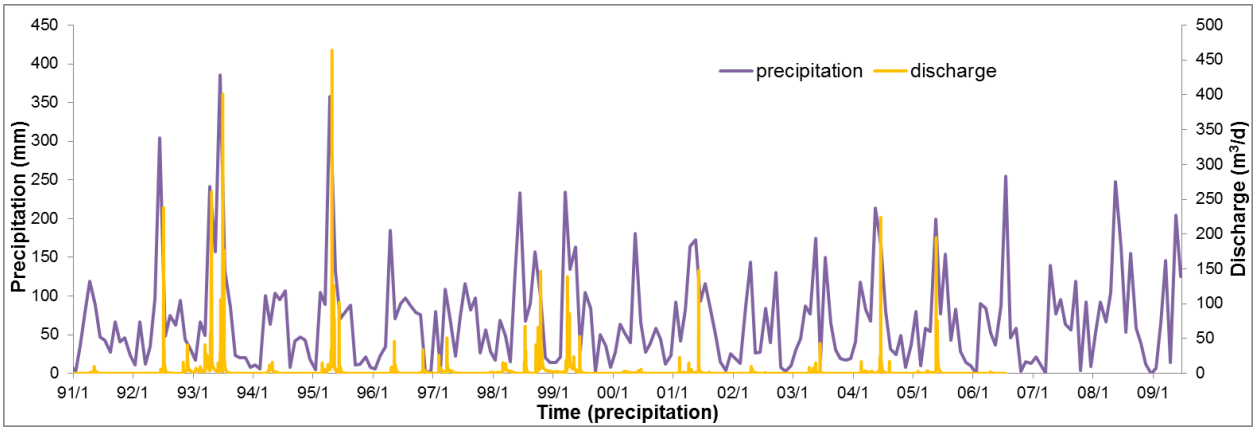


**(a)**

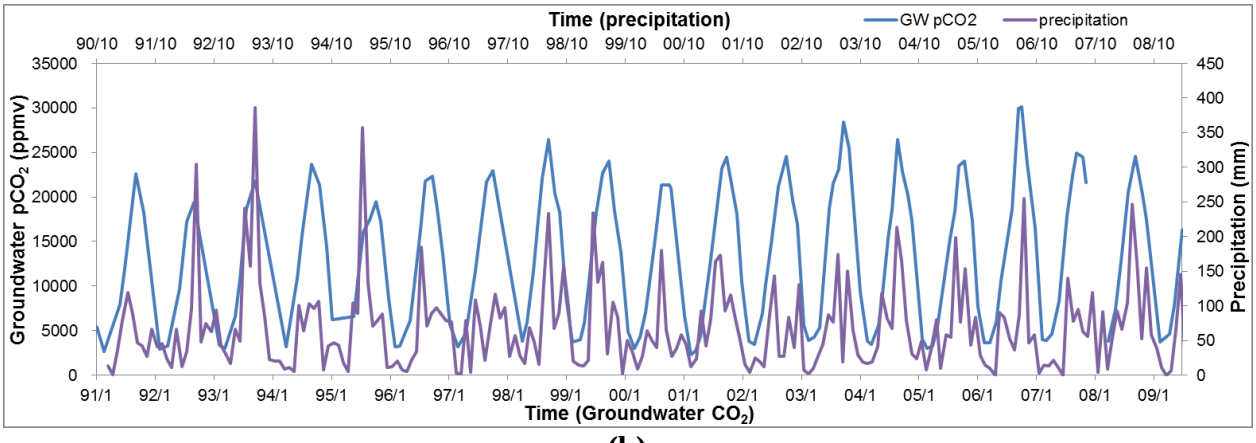


**(b)**

Figure C.5: Relation between precipitation and discharge of Kings Creek (USGS gauging station 06879650) (a), time-lagged groundwater $pCO_2$ and precipitation (b).

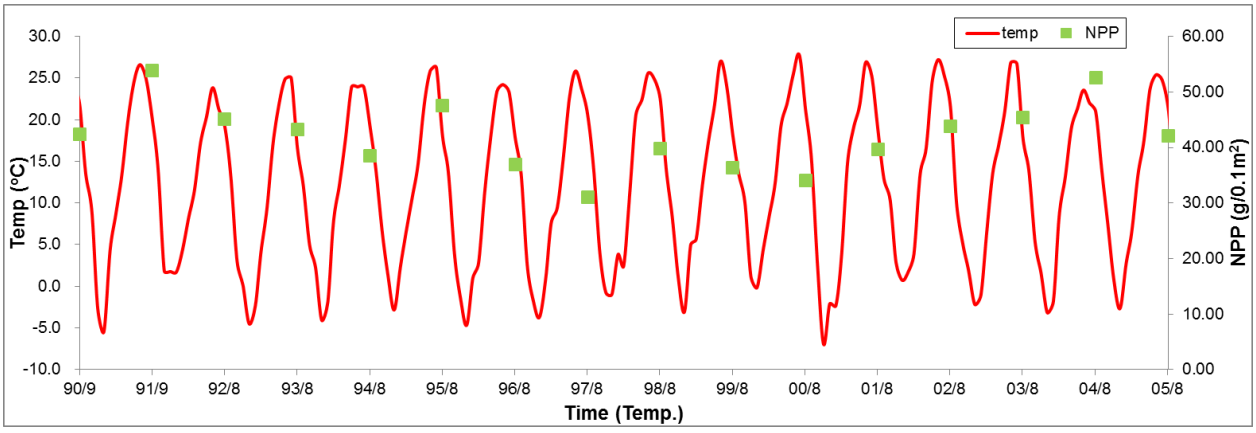


**(a)**

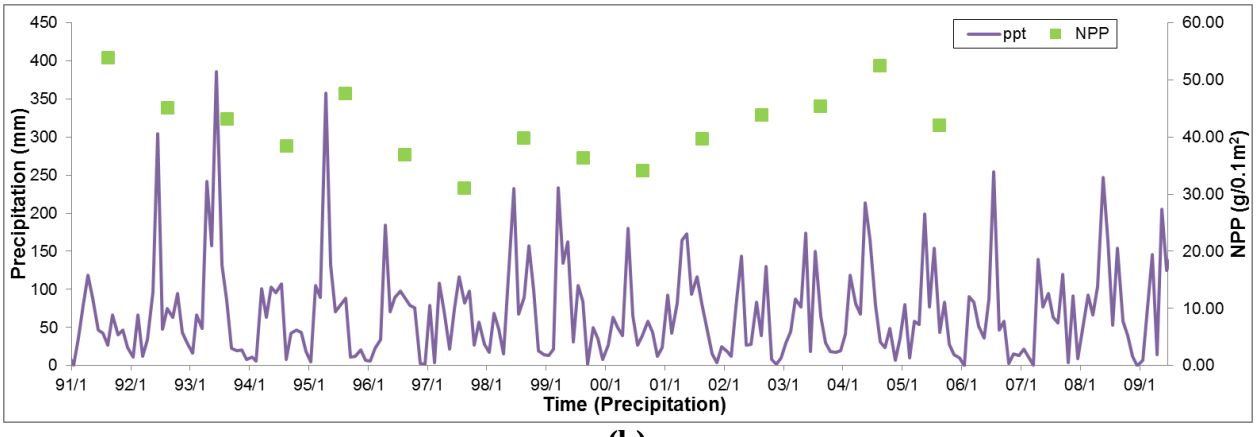


**(b)**

Figure C.6: Relation between temperature and net primary production (a), precipitation and net primary production (b).

**Appendix D. Geochemical speciation modeling results from PHREEQC**

For Konza May sampling, pH, DO and temperature along with laboratory-determined alkalinity, other anions, and cations were input in PHREEQC (Parkhurst and Appelo,1999) to calculate $CO_2$ partial pressure ($pCO_2$) and the calcite saturation index (SIc) for each record.

For Maolan sampling, water temperature, pH, DO, estimated $Ca^{2+}$ and $HCO_3^-$, with mean monthly values of $K^+$, $Na^+$, $Mg^{2+}$, $Cl^-$ and $SO_4^{2-}$ (resolutions are 0.01 mg/L), were speciated using PHREEQC to calculate $pCO_2$ and the SIc for each data set.

For the Konza Prairie long-term data, the full chemical analysis and SIc of well 3-5 and well 4-6 are input in PHREEQC to calculate the pH and the partial pressure of $CO_2$.

**References cited in all appendices**

Amthor, J.S., 1995. Terrestrial higher-plant response to increasing atmospheric [$CO_2$] in relation to the global carbon cycle. Global Change Biology 1, 243-274.

Andresen, L.C., Michelsen, A., Ambus, P., Beier, C., 2010. Belowground heathland responses after 2 years of combined warming, elevated $CO_2$ and summer drought. Biogeochemistry 101, 27-42.

Bond-Lamberty, B., Thomson, A., 2010. Temperature-associated increases in the global soil respiration record. Nature 464, 579–582.

Briones, M.J.I., Ostle, N.J., McNamara, N.P., Poskitt, J., 2009. Functional shifts of grassland soil communities in response to soil warming. Soil Biol. Biochem. 41, 315–322.

Buchanan, D.L., Corcoran, B.J., 1959. Sealed tube combustions for the determination of carbon-14 and total carbon. Anal. Chem. 31, 1635–1638

Buermann, W., Lintner, B.R., Koven, C.D., Angert, A., Pinzon, J.E., Tucker, C.J., Fung, I.Y., 2007. The changing carbon cycle at Mauna Loa Observatory. PNAS Environ. Sci. 104, 4249–4254.

Dodds, W.K., Evans-White, M.A., Gerlanc, N.M., Gray, L., Gudder, D.A., Kemp, M.J., Lopez, A.L., Stagliano, D., Strauss, E.A., Tank, J.L., Whiles, M.R., Wollheim, W.M., 2000. Quantification of the nitrogen cycle in a prairie stream. Ecosystems 3, 574–589.

Freeman, C.C., 1998. The flora of Konza Prairie: a historical review and contemporary patterns. In: Knapp, A.K., Briggs, J.M., Hartnett, D.C., Collins, S.L. (Eds.), Grassland Dynamics – Long-Term Ecological Research in Tallgrass Prairie. Oxford University Press, New York, 69–80.

Gray, L.J., Macpherson, G.L., Koelliker, J.K., Dodds, W.K., 1998. Hydrology and aquatic chemistry. In: Knapp, A.K., Briggs, J.M., Hartnett, D.C., Collins, S.L. (Eds.), Grassland

Dynamics – Long-Term Ecological Research in Tallgrass Prairie. Oxford University Press, New York, 159–176.

Hayden, B., 1998. Regional climate and the distribution of tallgrass prairie. In: Knapp, A.K., Briggs, J.M., Hartnett, D.C., Collins, S.L. (Eds.), Grassland Dynamics –Long-Term Ecological Research in Tallgrass Prairie. Oxford University Press, New York, 19–34.

Harmon, M.E., Ferrell, W.K., Franklin, J.F., 1990. Effects on carbon storage of conversion of old-growth forests to young forests. Science 247, 699-702.

Hendry, M.J., Mendoza, C.A., Kirkland, R.A., Lawrence, J.R., 1999. Quantification of transient $CO_2$ production in a sandy unsaturated zone. Water Resour. Res. 35, 2189–2198.

Johnson, W.C., Willey, K.L, Macpherson, G.L., 2007. Carbon isotope variation in modern soils of the tallgrass prairie: analogues for the interpretation of isotopic records derived from paleosols. Quat. Int. 162, 3–20

Kissing, K. R., Macpherson, G. L., 2006. Short-term water-level fluctuations and long-term water-level decline at the Konza Prairie—drought or vegetation?.Geol. Soc. Am. Absts. Progs. 3835.

Liu, Z., Li, Q., Sun, H., Wang, J., 2007. Seasonal, diurnal and storm-scale hydrochemical variations of typical epikarst spring in subtropical karst areas of SW China: soil $CO_2$ and dilution effects. J. Hydrol. 337, 207–223.

Macpherson, G. L.,1992. Ground-water chemistry under tallgrass prairie, central Kansas, USA. In Proceedings of the 7$^{th}$ International Symposium on Water–Rock Interaction, Park City, Utah, USA(eds. Y. K. Kharak and A. S. Maest). A.A. Balkema, Brookfield, 809–812.

Macpherson, G. L., 1996. Hydrogeology of thin limestones–the Konza Prairie LTER Site. J. Hydrol. 186, 191–228.

Macpherson G. L. (2004) Field vs. lab pH in remote wells, Konza Prairie LTER site, and implications for limestone weathering. In Proceedings of the 11th International

Symposium on Water–Rock Interaction, Saratoga Springs, New York, USA(eds. R. B. Wanty and R. R. Seal, II). A.A. Balkema, New York, 845–848.

Macpherson, G. L., Roberts J. A., Blair J. M., Townsend M. A., Fowle D. A., Beisner K. R. 2008. Increasing shallow groundwater $CO_2$ and limestone weathering, Konza Prairie, USA. Geochimica et Cosmochimica Acta, v. 72, i. 23, pp. 5581-5599.

Milly, P.C.D., Wetherald, T.R., Dunne, K.A., Delworth, T.L., 2002. Increasing risk of great floods in a changing climate. Nature 415, 514 – 517.

Oviatt, C. G., 1998. Chapter 3 geomorphology of Konza Prairie. In Grassland Dynamics (eds. A. K. Kn app, J. M. Briggs, D. C. Hartnett and S. L. Collins). Oxford Univ. Press, New York, pp. 35–47.

Parkhurst, D., L., and Appelo, C., A., J., 1999. User's guide to PHREEQC (Version 2)—a computer program for speciation, batch-reaction, one-dimensional transport, and inverse geochemical calculations.U.S. Geol. Surv. Wat.-Resour. Investigations Report 99-4259, p. 312.

Pomes, M.L., 1995. A study of the aquatic humic substances and hydrogeology in a prairie watershed, use of humic material as a tracer of recharge through soils. Ph.D. thesis, Univ. Kansas

Ransom, M.D., Rice, C.W., Todd, T.C., Wehmueller, W.A., 1998. Soils and soil biota. In: Knapp, A.K., Briggs, J.M., Hartnett, D.C., Collins, S.L. (Eds.), Grassland Dynamics – Long-Term Ecological Research in Tallgrass Prairie. Oxford University Press, New York, pp. 48–66.

Reiners, W.A., 1972. Structure and energetics of three Minnesota forests. Ecological Monographs 42, 71-94.

Runyon, J., Waring, R.H., Goward, S.N., Welles, J.M., 1994. Environmental limits on net primary production and light-use efficiency across the Oregon transect. Ecological Applications 4, 226-237.

Sala, O.E., Parton, W.J., Joyce, L.A., Lauenroth, W.K., 1988. Primary production of the central grassland region of the United States. Ecology 69, 40-45.

Schulte, P., Geldern, R., Freitag, H., Karim, A., 2011. Applications of stable water and carbon isotopes in watershed research: Weathering, carbon cycling, and water balances. Earth-Sci. Rev., 109, 20-31.

Singh, J.S., Lauenroth, W.K., Steinhorst, R.K., 1975. Review and assessment of various techniques for estimating net aerial primary production in grasslands from harvest data. Botanical Review 41, 181-232.

Tate, K. R., and Ross, D. J., 1997. Elevated $CO_2$ and moisture effects on soil carbon storage and cycling in temperature grasslands. Glob. Change Biol.3, 225–235.

Thomas, R.B., Lewis, J.D., and Strain, B.R., 1994. Effects of leaf nutrient status on photosynthetic capacity in loblolly pine seedlings grown in elevated atmospheric CO2. Tree Physiology 14, 947-960.

Towne, E.G., 2002. Vascular plants of Konza prairie biological station: an annotated checklist of species in a Kansas tallgrass prairie. Sida 20, 269–294.

Tsypin, M., and Macpherson, G.L., 2012. The effect of precipitation events on inorganic carbon in soil and shallow groundwater, Konza Prairie LTER Site, NE Kansas, USA. Applied Geochemistry 27, 2356–2369.

Twiss, P.C., 1988. Beattie limestone (lower Permian) of eastern Kansas. In: Hayward, O.T. (Ed.), G.S.A. Centennial Field Guide, vol. 4, South-Central Section of the Geological Society of America. Geol. Soc. Am., 35–41.

Vinter, M. A. and I. C. Burke, 1997. Contingent effects of plant species on soils along a regional moisture gradient in the Great Plains. Oecologia 110, 393-402.

Wehmueller, W.A., Campbell, H.V., Hamilton, V.L., Graber, S.P., 2005. Soil survey of Geary County, Kansas. US Dept. of Agriculture, Natural Resources Conservation Service.

White, W. B., 1969. Conceptual models for carbonate aquifers. Ground Water 7, 15–21.

Zeller, D.E. (Ed.), 1968. The Stratigraphic Succession in Kansas. Kansas Geol. Survey Bull. 189.